Molecular Psychiatry (2019) 24:1748–1768
https://doi.org/10.1038/s41380-018-0065-x

ARTICLE

Pathogenic variants in E3 ubiquitin ligase RLIM/RNF12 lead to a syndromic X-linked intellectual disability and behavior disorder

Suzanna G. M. Frints[1,2] · Aysegul Ozanturk[3] · Germán Rodríguez Criado[4] · Ute Grasshoff[5] · Bas de Hoon[6,7] · Michael Field[8] · Sylvie Manouvrier-Hanu[9,10] · Scott E. Hickey[11,12] · Molka Kammoun[13] · Karen W. Gripp[14] · Claudia Bauer[5] · Christopher Schroeder[5] · Annick Toutain[15,16] · Theresa Mihalic Mosher[11,12,17] · Benjamin J. Kelly[17] · Peter White[12,17] · Andreas Dufke[5] · Eveline Rentmeester[6] · Sungjin Moon[3] · Daniel C Koboldt[12,17] · Kees E. P. van Roozendaal[1,2] · Hao Hu[18] · Stefan A. Haas[19] · Hans-Hilger Ropers[18] · Lucinda Murray[8] · Eric Haan[20,21] · Marie Shaw[20] · Renee Carroll[20] · Kathryn Friend[22] · Jan Liebelt[21] · Lynne Hobson[22] · Marjan De Rademaeker[23] · Joep Geraedts[1,2] · Jean-Pierre Fryns[13] · Joris Vermeesch[13] · Martine Raynaud[15,16] · Olaf Riess[5] · Joost Gribnau[6] · Nicholas Katsanis[3] · Koen Devriendt[13] · Peter Bauer[5] · Jozef Gecz[20,24] · Christelle Golzio[3,25] · Cristina Gontan[6] · Vera M. Kalscheuer[26]

Received: 23 November 2017 / Accepted: 28 February 2018 / Published online: 4 May 2018

Abstract

RLIM, also known as RNF12, is an X-linked E3 ubiquitin ligase acting as a negative regulator of LIM-domain containing transcription factors and participates in X-chromosome inactivation (XCI) in mice. We report the genetic and clinical findings of 84 individuals from nine unrelated families, eight of whom who have pathogenic variants in *RLIM* (RING finger LIM domain-interacting protein). A total of 40 affected males have X-linked intellectual disability (XLID) and variable behavioral anomalies with or without congenital malformations. In contrast, 44 heterozygous female carriers have normal cognition and behavior, but eight showed mild physical features. All *RLIM* variants identified are missense changes co-segregating with the phenotype and predicted to affect protein function. Eight of the nine altered amino acids are conserved and lie either within a domain essential for binding interacting proteins or in the C-terminal RING finger catalytic domain. In vitro experiments revealed that these amino acid changes in the RLIM RING finger impaired RLIM ubiquitin ligase activity. In vivo experiments in *rlim* mutant zebrafish showed that wild type RLIM rescued the zebrafish *rlim* phenotype, whereas the patient-specific missense *RLIM* variants failed to rescue the phenotype and thus represent likely severe loss-of-function mutations. In summary, we identified a spectrum of *RLIM* missense variants causing syndromic XLID and affecting the ubiquitin ligase activity of RLIM, suggesting that enzymatic activity of RLIM is required for normal development, cognition and behavior.

Introduction

The X-linked *RLIM* gene, also known as *RNF12*, encodes a widely expressed RING (Really Interesting New Gene) domain-containing zinc-finger protein with diverse cellular functions. This protein serves as a cofactor promoting or inhibiting transcription factor activity and acts as an E3 ubiquitin ligase ubiquitinating its target proteins for subsequent degradation by the proteasome [1, 2]. In humans, rare nucleotide changes in *RLIM* (MIM 300379) were identified recently in four families with X-linked intellectual disability (XLID) [3, 4], with clinical information reported for one family [4] and for a second family published in Spanish [5]. While our current understanding of the

These authors contributed equally: Suzanna G.M. Frints, Aysegul Ozanturk.

These authors jointly supervised this work: Christelle Golzio, Cristina Gontan, Vera M. Kalscheuer.

Electronic supplementary material The online version of this article (https://doi.org/10.1038/s41380-018-0065-x) contains supplementary material, which is available to authorized users.

✉ Suzanna G. M. Frints
s.frints@mumc.nl

✉ Vera M. Kalscheuer
kalscheu@molgen.mpg.de

Extended author information available on the last page of the article

functions of human *RLIM* is sparse, its mouse ortholog (*Rlim*/*Rnf*12) has been studied in vitro [6, 7] and in vivo [6, 8]. RLIM binds to LIM-homeodomain (LIM-HD) transcription factors and their cofactors CLIM (also known as NLI, Ldb, and Chip). It was identified as a negative regulator of LIM-HD transcription factors, acting either as a co-regulator via the recruitment of the Sin3A/histone deacetylase corepressor complex, or by targeting the cofactors for proteasomal degradation [8, 9]. Subsequent studies showed that in the mouse and *Xenopus* RLIM/Rlim is an important protein involved in early embryogenesis [10–12], e.g., lung, brain, and neural tube development [13]. In addition, mouse RLIM activates X-chromosome inactivation (XCI) [14–16]. In vitro studies in embryonic stem cells indicated that RLIM targets the XCI inhibitor REX1 for proteasomal degradation via polyubiquitination [2], and that at least one functional copy of *Rlim* is required to reduce REX1 levels sufficiently for initiation of XCI [17]. Furthermore, in mammalian cells RLIM is involved in telomere length homeostasis, promoting the ubiquitination of TRF1 [18]. RLIM plays a role in cell proliferation through the targeted degradation of stathmin [19]; upregulation of the p53 pathway through ubiquitination of MDM2 and proteasomal dependent degradation [20] and inhibiting the transcriptional activity of c-Myc through polyubiquitination of the c-Myc protein [6]. RLIM may thus act as a tumor suppressor on p53 and c-Myc. The range of RLIM functions extends further, primarily through its role in the ubiquitination of diverse substrates. RLIM is a positive regulator in the TGF-beta family signaling pathway. It affects cell migration by ubiquitinating the negative regulator Smad7 [11] and through its direct binding to the E3 ubiquitin-protein ligase SMURF2 [21]. Furthermore, RLIM affects expression of estrogen responsive genes through ubiquitination [22] and phosphorylation [23] of estrogen receptor alpha [6, 12, 22, 23] and hereby regulates its biological activity together with its cofactor CLIM in primary breast cancer tumor cells [22]. RLIM is a critical survival factor for mammary gland milk-producing alveolar cells [22].

Here we describe the recognizable and behavioral clinical phenotype of nine RLIM-affected families, including the evolving phenotype in affected males. All heterozygous carrier females have normal cognition and behavior, but a few have physical features, including mainly minor skeletal abnormalities. In vitro functional assays showed that patient-specific single amino acid substitutions located in the C-terminal RING-H2 zinc finger domain of RLIM led to decreased ubiquitin ligase activity. In vivo functional studies in zebrafish revealed that lack of *rlim* caused microcephaly and that none of the patient-specfic *RLIM* missense variants rescued this phenotype. Taken together, our genetic and functional data suggest that these *RLIM* missense variants are most likely causative for the clinical phenotype in the respective families.

Materials and methods

General workup

For all families, except Family E, at least the index patient was tested initially for karyotype, *FMR1* CGG repeat expansion and by microarray copy number variant analysis; and the results were normal except for one affected male (C.IV:2) who carried an 8q21.3 (1.1 Mb) duplication of unknown clinical significance. Families D (D072), F (MRX61/T11), and H (AU31) (Fig. 1) were part of our previous study on 405 families with unresolved XLID. *RLIM* variants identified in these families were reported earlier with limited clinical information [3, 5]. Family B, included in the clinical assessment and functional assays reported here, has been published before [4]. Families C, D, and F have been revisited and/or were reevaluated clinically. All families were evaluated by a clinical geneticist and/or pediatrician (for more clinical details see Supplementary text). The study was approved by the review boards of the participating institutions. Written informed consent of the included individuals was obtained from their parents or legal guardians.

Next-generation sequencing

Genomic DNA was isolated from peripheral blood and/or skin fibroblasts according to standard procedures. Next-generation sequencing was performed at different centers according to standard procedures. Trio based whole exome sequencing (WES) was performed in Family A on a clinical basis as described in Retterer et al. [24]. Index patients from Families C, D, F, and H were investigated by X-chromosome exome sequencing. Reads were mapped to the human reference genome hg18 via Razers [25] called with the following options: -mcl 25 -pa -m 1 -dr 0 -i 93 -s 11010111100110001011 1 -t 4 -lm -id. The data were processed as described in Hu et al. [3], including a split-read mapping approach (SplazerS [26]) and analysis of read depth to comprehensively call insertions and deletions. All detected sequence variants were lifted-over to genome version hg19 and functionally prioritized [3]. For Family E, whole genome sequencing (WGS) libraries were constructed using the Illumina TruSeq DNA PCR-Free Library Preparation Kit. Paired-end 150 bp reads were generated on an Illumina HiSeq 4000 to a minimum depth of 30× coverage. FASTQ files were generated and secondary data analysis was performed using Churchill, a pipeline that implements a best practices workflow for variant discovery and genotyping

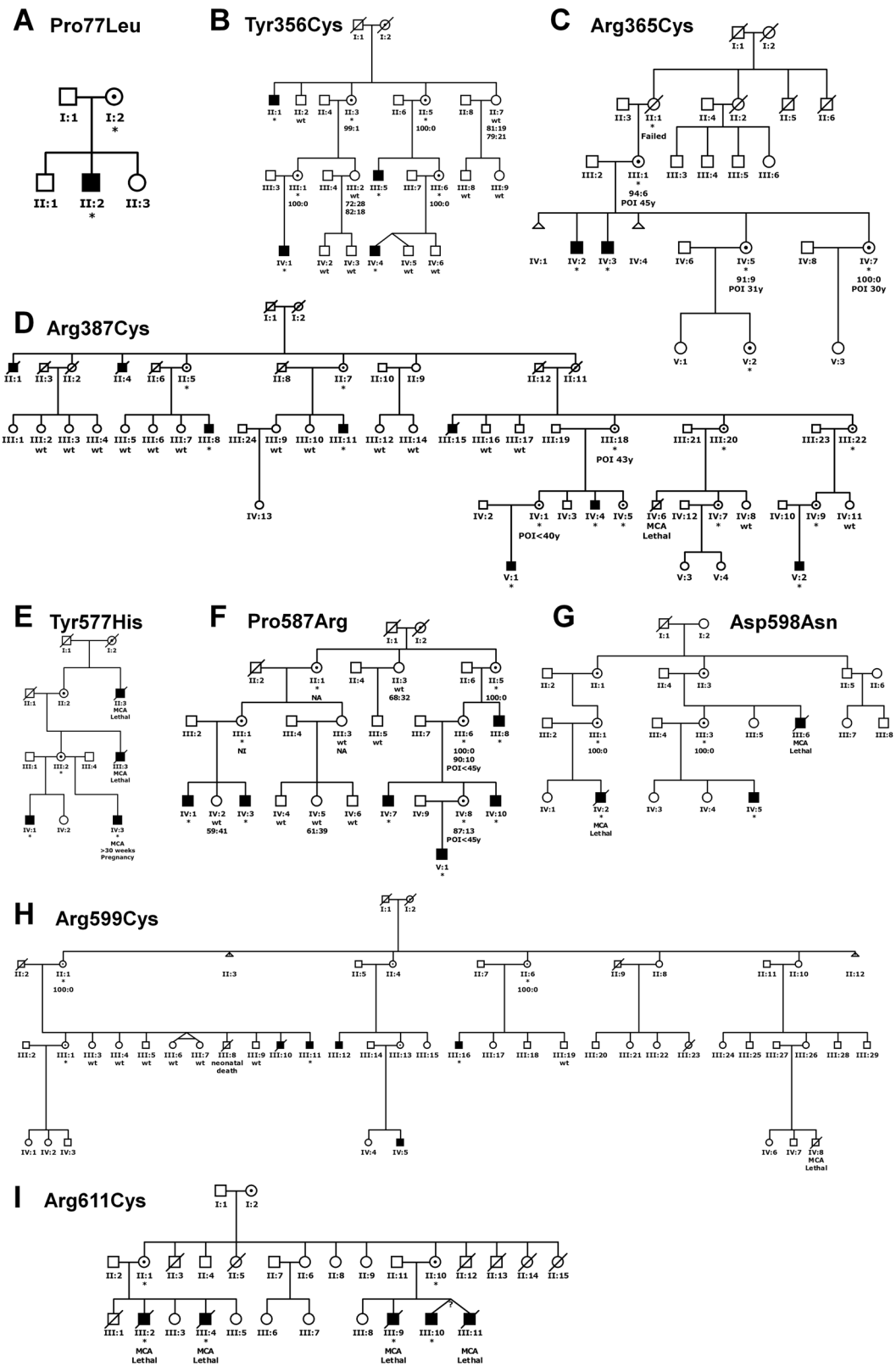

[27]. SNPeff, ANNOVAR, and custom in-house scripts were used to annotate the variant call set with mutation and gene information, protein functional predictions, and population allele frequencies. These annotations were used to identify rare (MAF <1% in ExAC) likely deleterious variants consistent with recessive inheritance (homozygous, compound

◀ **Fig. 1** Overview of *RLIM* families **A**–**i**. **A** USA: RLIM exon 4 c.230C>T, p.(Pro77Leu), **B** Norway: c.1067A>G, p.(Tyr356Cys)[4], **C** Australia AU38 c.1093C>T, p.(Arg365Cys), **D** Spain D072: c.1159C>T, p.(Arg387Cys), **E** USA: c.1729T>C, p.(Tyr577His), **F** France MRX61, T11: c.1760C>G, p.(Pro587Arg), **G** Belgium: c.1792G>A, p.(Asp598Asn), **H** Australia AU31: c.1795C>T, p.(Arg599Cys), and **I** Germany: c.1831C>T, p.(Arg611Cys). The *RLIM* mutation nomenclature was based on NCBI reference sequence NM_183353.2. Filled square: affected male. Dot in circle: (obligate) carrier female. *indicates that the *RLIM* variant was present. Wt: wild type allele present, familial *RLIM* variant absent. Skewed X-inactivation pattern in blood lymphocyte DNA in the *RLIM* carrier females shows nonrandom favorable inactivation of the mutant allele. Results were not interpretable for F.II:1, F.III:1, F.III:3; random X-inactivation profiles in B.II:7, B.III:2, F. II:3, F.IV:2 and F.IV:5 who are all noncarriers. POI premature ovarian insufficiency. MCA lethal: in most cases a lethal type of congenital diaphragmatic hernia with associated lung hypoplasia was present with mild growth retardation of prenatal onset, facial dysmorphism, (relative) microcephaly and hypogenitalism including micropenis with absent or small testes, cryptorchidism and/or hypospadias with limb anomalies, e.g., short terminal phalanges, preaxial polydactyly, hypoplastic absent or short nails (See also Supplementary Figures 2 and 4).

heterozygous or X-linked hemizygous variants). No high confidence de novo coding variants were detected. The resulting 20 variants affecting 15 genes (four homozygous recessive, eight compound heterozygous, and three X-linked hemizygous) were reviewed by the Rare Disease Genomics Board (an internal case review committee at Nationwide Children's Hospital, USA). For Family G, WES was performed for the two affected male cousins (G.IV:2 and G.IV:5) on a Hiseq2000. One hundred base pair paired-end reads were aligned to the reference genome using Burrows–Wheeler aligner. The quality metrics for mapping were calculated with Picard. Genome Analysis Toolkit framework was used for local realignment. Variants were annotated with Annovar. Total mapped reads number varied from 80, 721, 383 to 121, 928, 698 for the two samples with a minimum mean coverage at each target of 76 reads. On average, 93.8% of the bases were covered by at least 10 reads and 81% of the bases reached at least 30× sequence coverage. Variants were filtered based on their frequency and protein effect with exclusion of variants with MAF ≥0.01 in public databases for synonymous variants. Exome sequencing revealed shared rare variants in *RAB40A* and *RLIM*. The variant in *RAB40A* (NM_080879: c.A485G: p.(Asn162Ser)) has a minor allele frequency of 0.0014 in gnomAD (300/200128) and is present in 108 hemizygous and one homozygous individuals which makes it likely a benign variant. For family I, WGS was performed in the proband (III:10) and the parents (II:10, II:11), one aunt (II:1), and one uncle (II:2) underwent WES. The sequencing library for WGS was prepared using the Nextera DNA Library Preparation Kit (Illumina, San Diego) and sequenced on a HiSeq2500 (Illumina, San Diego) to an average depth of 17 times. All WES experiments were run on a GAIIx (Illumina, San Diego) after enrichment using the SeqCap EZ v2 enrichment kit (Roche, Pleasanton). The average mean depth of all WES was 91 times and 92% of all targets were covered with at least 10 times. On average 83, 723, 779 reads were generated per WES and 477, 781, 686 reads for WGS. Reads of all experiments were mapped using BWA (v.0.7.15), variants were called with freebayes (v.0.9.20 and 1.1.0) and annotated with SnpEff/SnpSift (v.4.1c and 4.3i). In-house scripts were used for QC and further functional annotation. All variants were filtered according the following rules: (1) keep only variants on the X-chromosome since the family history suggested X-linked inheritance, (2) only variants hemizygous in proband, heterozygous in obligate female carriers but not present in the proband's father were kept, (3) all not coding/splicing variants were removed, and finally (4) all variants with an allele fraction of >1% in ExAC were removed. With this strategy four variants remained and were further analyzed by segregation analysis in other affected individuals (brother (III:9) and two cousins (III:2, III:4)).

Linkage and segregation analysis

For families D, F, and G, linkage analysis was performed as described [5, 28, 29]. For all families, segregation analysis was performed with primer pairs flanking the variants identified in the families. Primer sequences are available upon request.

X-inactivation studies

For X-inactivation studies, DNA extracted from blood lymphocytes and skin fibroblasts was analyzed for the methylation sensitive site of *FMR1* exon 1 [30] and/or the CAG repeat of the androgen receptor gene [31]. For more details see Supplementary Materials and Methods.

Functional studies of *RLIM* variants in cells

The coding sequences of human *RLIM* and *REX1* were amplified from human cDNA and cloned into the TOPO Blunt II vector (Invitrogen). *RLIM* mutation constructs were generated by PCR site-directed mutagenesis. For mammalian expression, the wild type (WT) and the mutant *RLIM* coding sequences were subcloned into pCAG-FLAG (gift from D. van den Berg), a CAG-driven expression vector containing a FLAG-tag; *REX1* was subcloned into pCAG-FLAG-V5 vector.

HEK293 cells were cultured under standard conditions with 50% DMEM/50% Ham's F10, supplemented with 15% heat inactivated fetal calf serum, 100 U/ml penicillin, 100 mg/ml streptomycin, nonessential amino acids. For the ubiquitination assay, cells grown in 10 cm dishes were transiently transfected with polyethylenimine (Polysciences Inc.) for 48 h

with 3 µg WT or mutant RLIM expression vectors, in the absence or presence of 3 µg V5-tagged REX1 expression vector. Where indicated, cells were treated with 15 µM proteasome inhibitor MG132 (Sigma) for 3 h before harvesting.

Cells were collected by scraping on ice-cold PBS plus protease inhibitor (Roche). To isolate nuclear extracts, cells were incubated with 400 µl buffer containing 10 mM Hepes, 1.5 mM $MgCl_2$, 10 mM KCl, 0.5 mM DTT, protease inhibitor, and 15 µM MG132 for 10 min on ice. After vortexing briefly, nuclei were resuspended in buffer containing 20 mM Hepes, 25% glycerol, 420 mM NaCl, 1.5 mM $MgCl_2$, 0.2 mM EDTA, 0.5 mM DTT, protease inhibitor and 15 µM MG132 and incubated for 20 min on ice. After centrifugation, the supernatant was used as nuclear extract. For immunoblotting 20 µg of nuclear extract was used and detected with antibodies against RLIM (B01P, Abnova), V5 (Invitrogen), and β-ACTIN (Sigma) was used as a loading control. To recover V5-tagged REX1 15 µl of V5 antibody-agarose beads (Sigma) were added to nuclear extracts and the mixture was incubated for 2 h at 4 °C. The beads were washed with buffer containing 20 mM Hepes, 10% glycerol, 150 mM KCl, 1.5 mM $MgCl_2$, 0.2 mM EDTA, 0.02% NP40, 0.5 mM DTT, protease inhibitors, and 15 µm MG132. Bound proteins were eluted with sample buffer and visualized by immunoblotting. Co-immunoprecipitated RLIM was detected with RLIM antibody, and poly-ubiquitinated REX1 with a V5 antibody.

Knockdown of *rlim* in zebrafish, rescue experiments, staining, and embryo manipulation

Zebrafish embryos were raised as described [32]. All animal experiments were carried out with the approval of the Institutional Animal Care and Use Committee. A splice-blocking morpholino (sb-MO) against the third exon–intron junction of *rlim:* (5′-CTGTCGCTGGGAATGACAA-GAAATT-3′) was designed and purchased from Gene Tools. For RNA rescue experiments, human WT *RLIM* DNA (NM_183353.1) was obtained from Open Biosystems (Clone ID: 3834870) and cloned into a pCS2+ vector. The seven patient-specific missense changes, p.(Pro77Leu), p.(Tyr356Cys), p.(Arg365Cys), p.(Arg387Cys), p.(Pro587Arg), p.(Arg599Cys), p.(Arg611Cys), and the polymorphic p.(Asn178Thr) change which served as a control were introduced into the full-length *RLIM* construct by site-directed mutagenesis. In vitro transcription of WT and mutant constructs was performed using the SP6 Message Machine kit (Ambion). The *rlim* sb-MO (2 ng) and *RLIM* WT or mutant RNA (100 pg) were injected into zebrafish embryos at one- to two-cell stage. Morpholino efficiency was determined by RT-PCR. Total RNA was extracted from 2 day-old embryos using TRIzol® Reagent (Life Technologies). First-strand cDNA was synthesized using Superscript® III with oligo(dT) primer and PCR amplification was carried out using zebrafish *rlim* primers (Forward, 5′-GAACCGACTTAGGCAGGTCA-3′ and Reverse, 5′-AAGGTTGATCGGTGAACGAC-3′). Injected embryos were scored at 5 days post-fertilization (dpf) for head area measurement. For staining, embryos were fixed in 4% PFA overnight. After gradual rehydration, embryos were treated with a bleach solution (1% H_2O_2, 0.1% KOH in 1% PBS) and stained with Alcian Blue solution (1% HCl, 70% EtOH, 1% Alcian blue). Embryos were cleaned with acidic ethanol (5% HCl, 70% EtOH) and imaged in 100% glycerol. All images were acquired on a Nikon macroscope. *T*-test was performed to determine significance between the tested conditions. Investigator was blinded when assessing the outcome and no method of randomization was used.

Generation and validation of *rlim* guide RNA (gRNA)

A gRNA was designed to target exon 1 of *rlim* as described [33]. Oligonucleotides (Forward, 5′-TAGGTCAGGA-TAATGCAGATCA-3′ and Reverse, 5′-AAACTGATCTG-CATTATCCTGA-3′) annealed and cloned into pT7Cas9sgRNA vector (Addgene) by *Bsm*BI. Template DNA was linearized by *Bam*HI and purified by phenol/chloroform extraction. Then the gRNA was in vitro-transcribed with MEGAshortscript T7 kit (Invitrogen). Subsequently, gRNA (100 pg) and Cas9 (200 pg) protein (PNA bio, CP01) were directly injected into one-cell stage embryos. For the efficiency of gRNA, genomic DNA from each embryo (F0) was extracted by proteinase K digestion (Life technologies, AM2548). By using a primer set (Forward, 5′-TATTTTTCTCTCGATGCGTGTG-3′ and Reverse, 5′-TGAAAATTGTTTTTACCAGGGG-3′) flanking the targeted genomic editing site, the genomic region was amplified, followed by denaturing and slow reannealing to facilitate heteroduplex formation (denaturing step: 5 min, followed by reannealing step: cooling to 85 °C at −2 °C/s and additional to 25 °C at −0.1 °C/s). The reannealed PCR amplicon was subjected to digestion by T7 endonuclease I (New England Biolabs, M0302L) at 37 °C for 1 h, and was resolved on 1.5% agarose gel. For the confirmation of genome editing at the *rlim* locus, PCR fragments were cloned into the pCR4/TOPO TA cloning vector (Life technologies, 450030), and each clone was Sanger sequenced; the percentage of mosaicism was determined and estimated at ~75% in the F0 population.

Results

RLIM-affected males have a recognizable and behavioral clinical phenotype

Pedigrees of the families studied and their *RLIM* variants are shown in Fig. 1. Affected males and carrier females

Table 1 Summary of the clinical features of 40 RLIM-affected males of Families A–I

Category	Subcategory	Features			
Reference ID	*RLIM*/RNF12 Phenotype	Males	$n = 40$ (three male fetuses, eight newborns, nine boys, 20 adults) Ranging from TOP at 21W of gestation till >80Y of age		
Gender					
Inheritance status	—		Affected males with X-linked RLIM defect		
Clinic present			Yes (% informative)	No (% informative)	Unknown/not applicable
Growth	Height	Short stature = <P3 (prenatally, childhood)	11 (79%)	3 (21%)	26/0
	Build	Normal stature (adulthood): length cm percentile	9 (64%)	5 (36%)	6/20
		Lean body build (child–adulthood)	17 (94%)	1 (6%)	9/13
		Central obesity (adulthood)	7 (54%)	6 (46%)	7/20
Head and neck	Head	Microcephaly (=<P3) OFC cm percentile	12 (86%)	2 (14%)	27/0
		Normocephaly (adulthood)	8 (62%)	5 (38%)	7/20
		Broad prominent high forehead (childhood)	17 (100%)	0 (0%)	21/2
	Face	Facial asymmetry	6 (24%)	19 (76%)	14/1
		Narrow face (adulthood)	11 (73%)	4 (27%)	5/20
		Long face (adulthood)	12 (80%)	3 (20%)	5/20
		Micrognathia	17 (68%)	8 (32%)	15/0
	Ears	Normal ears	22 (88%)	3 (12%)	15/0
		Normal hearing	20 (100%)	0 (0%)	9/11
	Eyes	Down-slanting palpebral fissures	20 (80%)	5 (20%)	15/0
		Hypertelorism (childhood)	12 (92%)	1 (8%)	27/0
		Hypotelorism (adulthood)	13 (93%)	1 (7%)	5/20
		Straight (lateral) eyebrows	23 (100%)	0 (0%)	16/1
		Synophrys	6 (26%)	17 (74%)	16/1
		Normal vision (includes correction with glasses)	20 (100%)	0 (0%)	9/11
	Nose	Broad nasal bridge (childhood)	17 (100%)	0 (0%)	23/0
		High nasal bridge (childhood)	19 (90%)	2 (10%)	19/0
		High narrow nasal bridge (adulthood)	15 (100%)	0 (0%)	5/20
		Beaked nose (adulthood)	5 (33%)	10 (66%)	5/20
	Mouth	Thin upper lip	22 (92%)	2 (8%)	16/0
		Small oropharynx including high narrow palate	6 (100%)	0 (0%)	34/0
		Velopharyngeal insufficiency—swallowing difficulties	8 (100%)	0 (0%)	21/11
		Downturned corners of the mouth	17 (89%)	2 (11%)	21/0
		Open mouth appearance (childhood)	6 (75%)	2 (25%)	21/11
	Teeth	Widely spaced	6 (60%)	4 (40%)	18/12
		Malar hypoplasia	8 (89%)	1 (11%)	19/12
Cardiovascular	Heart	Congenital heart defect	4 (17%)	19 (83%)	17/0
		Tetralogy of fallot	1	Not applicable	Unknown
		Atrial septal defect	1	Not applicable	Unknown
		Aortic stenosis	3	Not applicable	Unknown
		Other	1		
Respiratory	Lungs	Hypoplasia of lung(s)	10 (38%)	16 (62%)	13/0

Table 1 (continued)

Category	Subcategory	Features			
Reference ID	*RLIM*/RNF12 Phenotype	Males	$n = 40$ (three male fetuses, eight newborns, nine boys, 20 adults) Ranging from TOP at 21W of gestation till >80Y of age		
Gender					
Inheritance status	—		Affected males with X-linked RLIM defect		
Chest	Internal features	Congenital diaphragmatic hernia	11 (50%)	10 (50%)	19/0
Genitourinary	Genitalia	Small (micro) penis	9 (90%)	1 (10%)	30/0
		Small or absent testes	9 (82%)	2 (18%)	29/0
		Cryptorchidism	9 (82%)	2 (18%)	29/0
		Hypospadias	4 (40%)	6 (60%)	30/0
Skeletal	Hands	Short distal phalanges, e.g., thumbs	14 (88%)	2 (12%)	24/0
	Feet	Pes planus	6 (75%)	2 (25%)	32/0
Skin, nails, and hair	Nails	Short nails, nail hypoplasia, absent nails	5 (30%)	12 (26%)	23/0
Neurologic	Central nervous system	Intellectual disability (mild-moderate-severe)	29 (100%)	0 (0%)	11/0
		Delayed motor milestones	28 (97%)	1 (3%)	0/11
		Delayed speech (moderate to severe)	29 (100%)	0 (0%)	0/11
		Hypotonia (at birth), degree	8 (80%)	2 (20%)	28/2
		Drooling (childhood)	7 (100%)	0 (0%)	22/11
		Facial grimacing	8 (89%)	1 (11%)	20/11
		Broad-based gait	7 (88%)	1 (22%)	20/12
		Hyperreflexia	6 (100%)	0 (0%)	24/10
		Brisk reflexes	5 (100%)	0 (%)	25/10
		Other	7[a]		
	Behavioral psychiatric manifestations	Friendly/social (childhood)	13 (100%)	0 (0%)	16/11
		Shyness/quiet (child and adulthood)	12 (100%)	0 (0%)	17/11
		Loaner	10 (91%)	1 (9%)	18/11
		Verbal aggressiveness	11 (100%)	0 (0%)	18/11
		Self-injurious behavior, e.g., hand biting	5 (50%)	5 (50%)	17/13
		Outburst of anger/temper tantrums/ aggressiveness	12 (100%)	0 (0%)	17/11
		Anxiety	14 (93%)	1 (7%)	12/13
		Restlessness	12 (92%)	1 (8%)	14/13
		Autistic features or autism spectrum disorder	15 (88%)	2 (12%)	12/11
		Hyperactivity	5 (83%)	1 (17%)	23/11
		Decreased attention span	9 (90%)	1 (10%)	17/13
		Unhappy facial appearance	8 (73%)	3 (27%)	18/11
		Depressed mood	8 (73%)	3 (27%)	18/11
		Sleep disturbed	6 (55%)	5 (45%)	18/11
		Abnormal behavior not specified	8 (73%)	3 (27%)	17/12
		Other	0		
General	Social	Clinical variability present within the family	37 (100%)	0 (0%)	3/0
		Features in typical affected male include mild growth retardation (prenatal onset), intellectual disability, (relative)	20 (95%)	1 (5%)	8/11

Table 1 (continued)

Category	Subcategory	Features			
Reference ID	*RLIM*/RNF12 Phenotype	Males	$n = 40$ (three male fetuses, eight newborns, nine boys, 20 adults) Ranging from TOP at 21W of gestation till >80Y of age		
Gender					
Inheritance status	—		Affected males with X-linked RLIM defect		
		microcephaly (childhood), hypertelorism (childhood), hypogenitalism, hypotelorism (adulthood), and behavioral problems			
		Sheltered environment incl. free activities	22 (100%)	0 (0%)	5/11
	Death, cause of death	Congenital diaphragmatic hernia (CDH) Lung hypoplasia (LH)	1 LH, 2 CDH, 7 CDH-LH	20	9/0
		Other	Two TOP, two unknown, one Alzheimer dementia, one car accident		
Molecular basis	Conventional karyotype	Normal	6	0	34/0
	Molecular karyotype	Normal	4	1	35/0
	Whole genome exome, X-exome, *RLIM* Sanger sequencing	Ring finger protein, LIM domain interacting; RLIM/RNF12; OMIM *300379 proven defect	27	0	13 not tested

[a]Stiff gait (three times, poor balance, meningitis age 3 years; totally paralyzed, tension headache, cerebrovascular accident (hemorrhagic stroke) at age 28Y left hemiplegia with complete recovery, incontinence for urine and feces

were assessed clinically using a scoring list. Clinical symptoms present in at least five unrelated affected males are summarized in Table 1 with more details provided in the Supplementary text and in Supplementary Table 2. Clinical information on affected carrier females is presented in Supplementary Table 3. For the affected males, clinical data were obtained for 40 subjects, including three fetuses (Fig. 1 ongoing >30 weeks pregnancy of E.IV.3 with an affected male fetus, G.IV:2 was a termination of pregancy (TOP) at 21 weeks of gestation and I.III:9 was a TOP at 30 weeks of gestation), eight deceased newborns (Fig. 1, D. IV:6, E.II:3, E.III:3, G.III.6, H.IV:8, I.III:2, I.III:4, I.III.11), nine boys (Fig. 1, A.II:2, B.IV:1, B.IV:4, D.V:2, E.IV:1, F. V:1, G.IV:5, H.IV:5, I.III.10), and 20 adults (Fig. 1, B.II:1, B.III:5, C.IV:2, C.IV:3, D.II:1, D.II:4, D.III:8, D.III:11, D. III:15, D.IV:4, D.V:1, F.III:8, F.IV:1, F.IV:3, F.IV:7, F. IV:10, H.III:10, H.III:11, H.III:12, H.III:16).

Twelve of the 40 affected males (two fetuses and eight stillborns) died at birth because of multiple congenital malformations. The cause of death in 10/17 was congenital diaphragmatic hernia (CDH) with associated lung hypoplasia (LH) in 7/10 (G.IV:2, G.III:6, I.III:2, I.III:4, I.III:9, I. III:10, I.III:11), CDH without LH in 2/10 (E.II:3, E.III:3), and LH only in 1/10 (D.IV:6). One affected male fetus (ongoing pregnancy E.IV:3) had CDH and female appearing genitalia (male hypogenitalism) on ultrasound and fetal magnetic resonance imaging (MRI)-scan (Supplementary Figure 2 E.IV:3). One affected boy (G.IV:5) survived with a small CDH and mild LH. He presented with typical childhood features (Fig. 2, Supplementary Figure 2 and Supplementary Table 2).

Global developmental motor and speech delay, as well as ID, were reported for all 29 surviving affected males (29/40 = 73%). Cognitive dysfunction varied from borderline to severe ID. Speech delay and expressive language were of concern. In childhood, the boys were rather quiet and shy (12/12), presented with autistic-like features (15/17), and had an amiable social personality (13/13). In adolescence and adulthood significant behavioral problems were present. These included (hetero-) aggressive behavior including verbal aggressiveness (11/11), temper tantrums or outbursts of anger (12/12), anxiety (14/15), self-injurious behavior, e.g., hand biting (5/10), repetitive autistic or obsessive-compulsive like behaviors (15/17) and hyperactivity (5/6). In the adult-affected males (20/40), anxiety (14/15), abnormal behavior (8/11), and/or being unhappy or having depressed mood (8/11) with disturbed sleep (6/11) was reported. One affected male (C.IV:2) had a diagnosis of schizophrenia. Seizures were reported in three unrelated males (A.II:2, D. V:1, F.III:8) varying from infrequent seizures to well controlled with medication (e.g., Depakine). Seizure types included mainly absences (D.V:1, F.III:8), but a complex

partial seizure disorder was reported in one individual (A. II:2). Additional neurological signs in childhood were cerebral palsy (A.II:2), broad-based gait (7/8) with spastic gait (4/7), intention and/or rest (hand) tremor (3/5) increasing when anxious, drooling and swallowing difficulties. There was evolving lower limb spasticity in adulthood

◀ **Fig. 2** Evolution of RLIM defect-related facial dysmorphism from newborn until old age. Clinical data were obtained from 40 affected males: three fetuses (Fig. 1 ongoing >30 weeks pregnancy of E.IV.3, G.IV:2 termination of pregnancy (TOP) at 21 weeks and I.III:9 TOP at 30 weeks of gestation), eight deceased newborns (Fig. 1, D.IV:6, E. II:3, E.III:3, G.III.6, H.IV:8, I.III:2, I.III:4, I.III.11), nine boys (Fig. 1, A.II:2, B.IV:1, B.IV:4, D.V:2, E.IV:1, F.V:1, G.IV:5, H.IV:5, I.III.10), and 20 adults (B.II:1, B.III:5, C.IV:2, C.IV:3, D.II:1, D.II:4, D.III:8, D. III:11, D.III:15, D.IV:4, D.V:1, F.III:8, F.IV:1, F.IV:3, F.IV:7, F. IV:10, H.III:10, H.III:11, H.III:12, H.III:16). *RLIM* is a syndromic X-linked intellectual disability (XLID) gene with recognizable changing phenotype from newborn to adulthood (top panel) and from adulthood to old age (bottom panel). At birth growth retardation is present with microcephaly, broad high nasal bridge, hypertelorism, straight lateral eyebrows, and down-slanting palpebral fissures (D.V:1a–f at age 3 days (D3)–18 years (18Y), D.V:2a–c at age 0–4Y, E.IV:1a at age 1–2Y, F.IV:7a–d at age 6 months (6M)–5Y, G.IV:5a–c at age 3M–6Y, I.III:10a at age 5–6Y, D.V:4a–b at age 7–17Y, F.V:1a1–2 at age 9M, D.II.4a at age 2–3Y, D.II:1a at age 2–3Y, A.II:2a1–2 at age 6–7Y, F. IV:10a–c at age 6–15Y, D.III:11a–b at age 14–18Y, D.III:8a–b at age 14–20Y). The facial features in adults include long narrow face, narrow high nasal bridge, hypotelorism, and downturned corners of the mouth with sad looking appearance (F:IV:3a at age 26Y, F:IV:10 at age 26Y, F:IV:7e at age 32Y, F.IV:1a at age 32Y, F.III:8a at age 48Y, D:IV:4c at age 38Y, D.III:15a at 47Y, D.II:4b–c at age 43–73Y, D. III:11c at age 51Y, D.III:8c at 61Y, D.II:1b at 40Y, C.IV:2a at age 39Y and C.IV:3a at age 38Y)

(hyperreflexia (6/7) or brisk reflexes (1/7)). Progressive tetraplegia with Alzheimer type dementia was reported in one male (D.II:1). Brain abnormalities on neuroimaging/neuropathology were noted in three males across two families (3/8 tested individuals). However, the majority of males did not have neuroimaging and brain MRI was normal in 5/8 investigated males. Atypical white matter abnormalities were noted in childhood in three boys (Fig. 1, A.II:2, D.V:1, D.IV:4). One had periventricular leukomalacia, thin corpus callosum and pineal gland cyst (A.II:2); one had atypical white matter hypomyelinisation and pituitary gland hypoplasia (D.V:1) (Supplementary Table 2 and Supplementary Figure 5); and one had a spontaneous intracranial hemorrhage at age 28 years (D.IV:4), from which he recovered well.

Affected males from two families (Families F (MRX61) and H) had been considered previously as non-dysmorphic. However, following reassessment and comparison of their clinical features and photographs taken at various ages with affected males from unrelated families (Fig. 2), it became obvious that they had an evolving and recognizable clinical and behavioral phenotype.

Moreover, diseased newborns and boys with pathogenic *RLIM* variants, or a variant of unknown significance in the case of Family A with p.(Pro77Leu), had (mild) prenatal growth retardation/postnatal short stature (birth length <3rd percentile) (11/14) and dysmorphic features (17/40). Common facial dysmorphic features in childhood and adulthood (Fig. 2, upper panel) included microcephaly with broad prominent high forehead (16/16), broad nasal bridge (17/17), high nasal bridge (19/21), hypertelorism (12/13), straight eyebrows (23/23), synophrys (6/23), facial asymmetry (6/25), thin upper lip (22/24), malar hypoplasia (8/9), downturned corners of the mouth (17/19), open-mouthed appearance (6/8), small pointed chin and/or micrognathia (17/23), and widely spaced teeth (6/10). There were significant feeding difficulties during infancy, mainly as a result of velopharyngeal insufficiency and swallowing difficulties (8/8). A few affected males presented with a small oropharynx with high narrow palate (6/6) and one male (D.III:8) had a bifid uvula.

In adulthood (Fig. 2, lower panel) growth parameters were generally within the normal range (9/14). The faces became narrower (11/15) and longer (12/15) with a high narrow nasal bridge (15/15) and a prominent beaked nose in several males (5/15). Most were normocephalic (8/13) and had hypotelorism (13/14). Ears were mostly well-shaped (22/25) and hearing and vision were normal (20/20). Affected males had a lean body habitus (17/18). Adult males had truncal/central obesity (7/13).

Urogenital abnormalities included micropenis (9/10), cryptorchidism (8/10), small or absent testis (9/11 by ultrasound investigation), and hypospadias (4/10). In one child (G.IV:5) and one deceased newborn (I.III:2) cysts of the renal collection ducts were present. Abdominal features reported in a few males included omphalocele (2/23), liver cysts (E.IV:1 multiple liver cysts in left lobe and G.VI:2 multiple liver cysts with ductal plate malformation), polysplenia (I.III:2), and malrotation of bowel (I.III:9).

Hands showed short distal phalanges with broad stubby thumbs (14/16), camptodactyly (3/19), syndactyly (2/20), and nail hypoplasia or absent nails (5/17) (Supplementary Figures 2 and 4). Feet showed pes planus (6/8), preaxial polydactyly (3/20), and/or with (partial) cutaneous syndactyly (3/13) (Supplementary Figures 2 and 4).

Four affected males had congenital heart defects (CHD) (4/23), two with aortic stenosis (D.III:11, D.V:1), one with aortic isthmus stenosis with persistent foramen ovale and an atrial septal with persistent left upper vena cava, isolated separation of vertebral artery) (I.III:10) and one with Tetralogy of Fallot (D.IV:4).

Cognition, behavior and facial phenotype were normal in the 44 heterozygous *RLIM* female carriers assessed (Supplementary Figure 3 and Supplementary Table 3). However, several female carriers were noted to have clinical or biochemical evidence of premature ovarian insufficiency (POI) (7/8). Nevertheless, carrier females of Family C conceived spontaneously, despite a paradoxically low AMH level. Clinical reevaluation of Family D revealed that female carriers had relatively short stature compared to their non-carrier sisters (Supplementary Figure 3), somewhat broad stubby thumbs with short distal phalanges (4/4 compared to

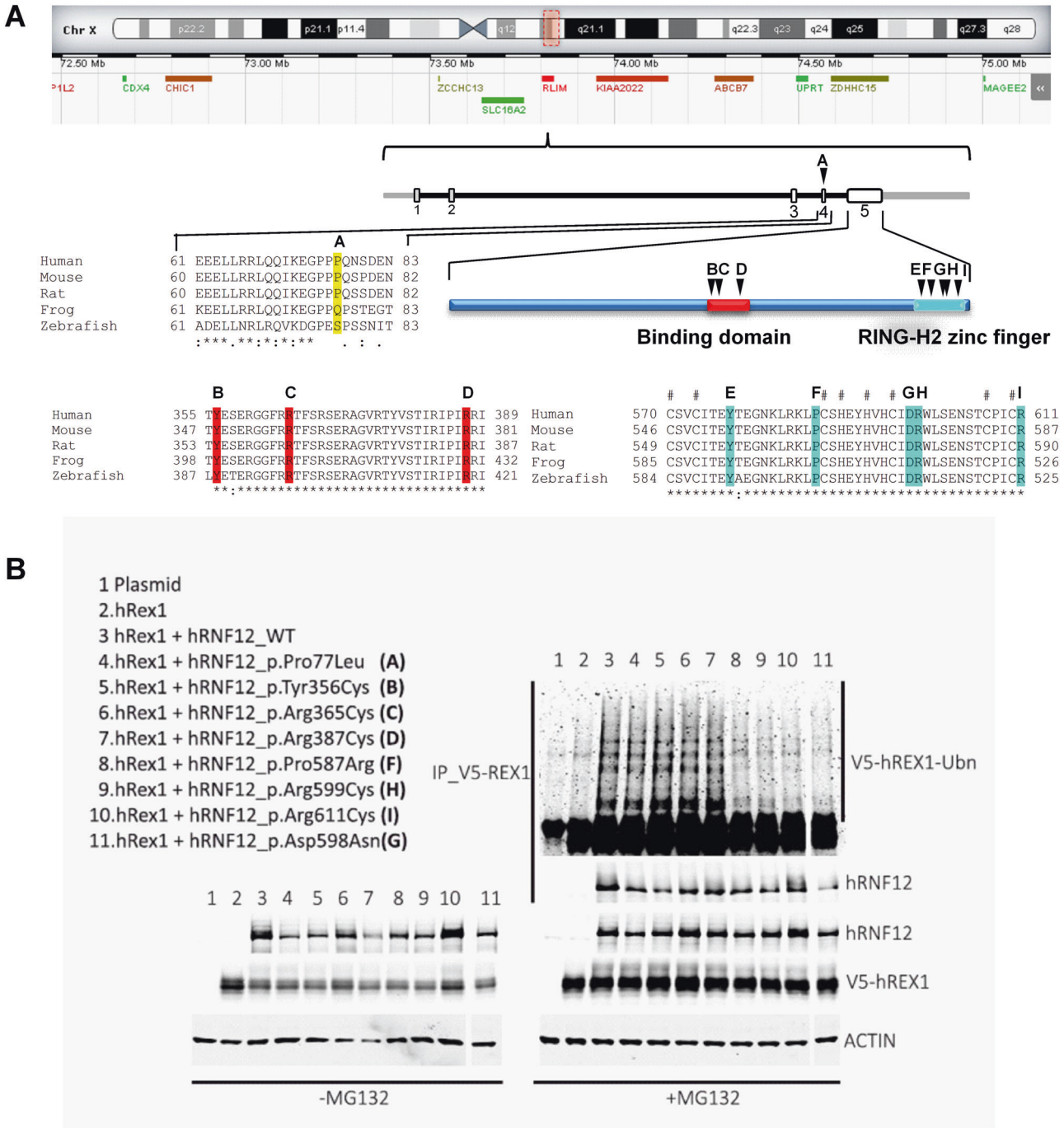

Fig. 3 Overview of *RLIM/RNF12* missense variants and ubiquitylation results using its established substrate REX1 in vitro. **A** Location of the *RLIM* gene on the X-chromosome and gene structure with missense variants identified in the families ((Family A with *RLIM* c.230C>T, p.(Pro77Leu) variant, Family B with c.1067A>G, p.(Tyr356Cys) variant, Family C with c.1093C>T, p.(Arg365Cys) variant, Family D with c.1159C>T, p.(Arg387Cys), Family E with c.1729T>C, p.(Tyr577His) variant, Family F with c.1760C>G, p.(Pro587Arg) variant, Family G with c.1792G>A, p.(Asp598Asn) variant, Family H with c.1795C>T, p.(Arg599Cys) variant and Family I with c.1831C>T, p.(Arg611Cys) variant, indicated by arrowheads), along with multiple alignments of the amino acid changes encoded by the pathogenic variants located in exon 5, which codes for the RLIM binding domain and the RING-H2 zinc finger domain. **B** In vitro ubiquitination assays in HEK293 cells. Left panels show nuclear protein extracts of HEK293 cells co-transfected for 48 h with the indicated expression constructs for V5-hREX1 in combination with RLIM (hRNF12) WT or with RLIM (hRNF12) mutant. Immunoblots were probed with the indicated antibodies. Right bottom panels show the same transfections, but HEK293 cells were treated with the proteasome inhibitor MG132 (15 µM) for 3 h prior to protein harvesting. Right upper panels: V5-tagged hREX1 was immunoprecipitated with anti-V5 agarose beads and analysed by immunoblotting to detect the poly-ubiquitinated hREX1 (hREX1-Ub_n) with V5 antibody. hRNF12 co-immunoprecipitated with hREX1 was detected with RLIM antibody. ACTIN was used as a loading control. Lanes 3 (hRNF12_WT) and 4 (Family A in Figs. 1 and 3A) show unaltered RLIM ubiquitination. Lanes 5, 6, and 7 (Families B, C, and D, respectively in Figs. 1 and 3a) show slightly increased RLIM ubiquitination compared to wild type, while lanes 8, 9, 10 and 11 (Families F, H, I, and G, respectively in Figs. 1 and 3A) show lower RLIM ubiquitination

0/3 noncarrier females) and pes planus (4/4 compared to 0/3 noncarrier females (Supplementary Figure 3). One young female carrier (Fig. 1 C.V:2) had unilateral choanal atresia and significant laryngomalacia requiring surgery.

Heterozygous *RLIM* female carriers have highly skewed XCI

XCI studies were performed on blood leukocytes or skin fibroblasts of fourteen heterozygous female carriers from five families (B [4], C, F, G, and H) and five noncarrier female relatives. While in thirteen female carriers XCI was (highly) skewed (90–100%), one female carrier showed less skewing (87%, F.IV:8). In contrast, five noncarrier female relatives had random XCI (between 61 and 81%, B.II:7, B. III:2, F.II:3, F.IV:2, F.IV:5) (Fig. 1 and data not shown). We investigated whether the *RLIM* variant in heterozygous female carriers was located on the inactive X-chromosome by performing more detailed studies on skin-derived fibroblast DNA and RNA from two females (C.IV:5 and C. IV:7). Methylation based X-chromosome inactivation ratio's (XIR) analysis confirmed skewed XCI in their fibroblasts (75.1 and 84.1%), although less pronounced than in their peripheral blood leukocytes (91 and 100%) (Supplementary Figure 6A). This difference could be due to acquired changes in the methylation pattern in fibroblasts during culturing, as RNA expression analysis for the X-chromosome encoded genes *HUWE1* and *NAP1L3* confirmed that XCI in the skin fibroblasts was highly skewed, corresponding to the XIR observed in peripheral blood leukocytes. *RLIM* expression analysis revealed that the mutated allele was not expressed in the majority of cells (Supplementary Figure 6B), suggesting that in the carrier females the X-chromosome which carries the *RLIM* variant is preferentially inactivated.

RLIM locus and variant identification

In four families (C, D, F, and H) the *RLIM* missense variants were identified by X-chromosome exome sequencing, in two families (A, G) by WES, and in two families (E, I) by WGS. In three families linkage analysis was performed. For Family D the maximum LOD score was 2.0 with the gene locus between Xp11.23 and Xq21.32 [5]. For Family G haplotype analysis using SNP arrays in two affected and five healthy males showed that the affected males share an X-linked region spanning 23.14 Mb, between markers rs4986622 and rs980114, with a maximum LOD score of 1.8. In these families the corresponding X-chromosome regions encompassed the *RLIM* gene.

All missense variants co-segregated with the phenotype (Fig. 1) and except for one variant (Family A, p.(Pro77-Leu)) located in exon 4, they clustered in exon 5 and altered highly conserved amino acids of the RLIM putative basic binding domain (Families B-D) or of the C-terminal catalytic RING-H2 zinc finger (Families E–I) (Fig. 3A and Supplementary Figure 1). Contrary to these disease-associated variants, the majority of *RLIM* missense variants reported in males in, e.g., gnomAD database, which is significantly depeleted of individuals with neurodevelopmental disabilities, are located outside these domains. The variants were predicted to affect function by in silico analysis including PolyPhen-2 and MutationTaster (see Supplementary Table 1). Except for the p.(Pro77Leu) substitution, which has been seen in eight heterozygous and two hemizygous individuals in gnomAD database (allele frequency of 5.812×10^{-5}), the variants identified in this study were not listed in publicly available databases. Combined the clinical, genetic and in silico data strongly suggested that these variants affect RLIM function.

Pathogenic RLIM variants alter its ubiquitin ligase activity in vitro

The protein regions of RLIM harboring the identified variants have not been functionally characterized, but the homologous regions in the mouse counterpart are highly conserved. In the mouse, the catalytic RING-H2 zinc finger is essential for poly-ubiquitinating its substrate REX1 (also known as ZFP42), leading to REX1 proteasomal degradation. *REX1* encodes a transcription factor, a member of the YY1 subfamily of cysteine-histidine (C2H2) zinc finger proteins. REX1 is considered to be a marker for mouse and human embryonic stem cells and is involved in XCI in the mouse [2]. Given the highly skewed XCI in the carrier females with heterozygous *RLIM* variants, we investigated whether these RLIM variants have an effect on REX1 ubiquitination by performing in vitro ubiquitination assays in HEK293 cells. Constructs encoding either FLAG-RLIM WT or one of the RLIM variants were co-transfected with V5-REX1. V5-REX1 pull-down was performed using anti-V5 antibody coupled beads from nuclear fractions pre-treated with the proteasome inhibitor MG132. Subsequent western blot analysis revealed that all RLIM mutants are able to bind REX1. However, there was a clear difference in the ubiquitin ligase activity between WT RLIM and four RLIM variants (Fig. 3B). Specifically, co-expression of tagged REX1 with the pathogenic RLIM variants p.(Pro587Arg) (Family F), p.(Asp598Asn) (Family G), p. (Arg611Cys) (Family I), and p.(Arg599Cys) (Family H), respectively, which map to the RING-H2 zinc finger, resulted in reduced REX1 ubiquitination (lanes 8, 9, 10, and 11 in Fig. 3B) when compared with WT RLIM (lane 3 in Fig. 3B), thus indicating that the corresponding mutant RLIM proteins have a reduced ubiquitin-protein ligase activity. In contrast, co-expression of the other RLIM

variants in the RLIM putative basic binding domain (p.(Tyr356Cys), Family B; p.(Arg365Cys), Family C; p.(Arg387Cys), Family D) resulted in slightly increased REX1 ubiquitination, suggesting that these variants lead to a slightly increased RLIM ubiquitin ligase activity (lanes 5, 6, and 7 in Fig. 3B) compared to WT RLIM (lane 3 in Fig. 3B). Finally, for the RLIM variant in the N-terminal region of the protein (Family A, p.(Pro77Leu) variant) (lane 4 in Fig. 3B) the ubiquitination activity was similar to the WT RLIM (lane 3 in Fig. 3B). These results suggest that

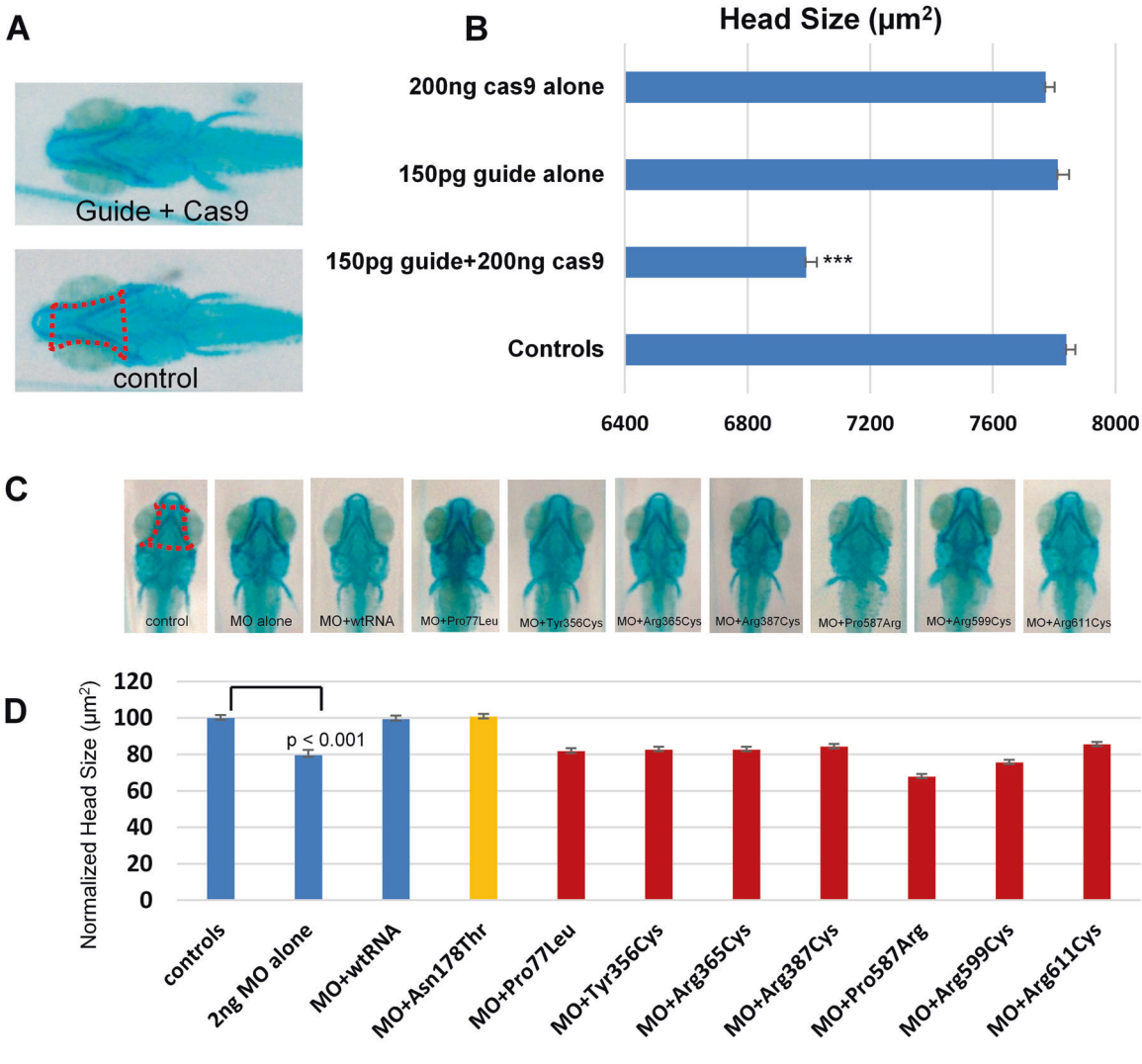

E

p-values	MO+wtRNA	MO+Asn178Thr	MO+Pro77Leu	MO+Tyr356Cys	MO+Arg365Cys	MO+Arg387Cys	MO+Pro587Arg	MO+Arc599Cys	MO+Arg611Cys
MO alone vs MO+RNAs	<0.001	<0.001	0.627	0.355	0.356	0.151	0.014 (null)	0.374	0.066
MO+wtRNA vs MO+mutantRNAs	-	0.125	<0.001	<0.001	<0.001	<0.001	<0.001	<0.001	<0.001

Fig. 4 Suppression of *rlim* results in microcephaly in zebrafish embryos. **A** Whole-mount Alcian blue staining of 5 dpf zebrafish embryos showing the cartilage structure in the head. Measured area for head size calculation is dotted with red in control. **B** Quantitative scoring of head size in embryos injected with guide + Cas9, guide alone, and Cas9 alone. Guide RNA + Cas9 injected batch showed 11% reduction (***p<0.001) in head size compared to controls. Guide RNA injected batch and Cas9 injected batch were not significantly different compared to the controls (n = 35–40 per batch, replicated). **C** Whole-mount Alcian blue staining of 5 dpf zebrafish embryos in MO rescue experiments. **D** Quantitative scoring of head size in embryos injected with MO alone, MO + wt RNA for rescue and MO + mutant RNA to test allele pathogenicity. Polymorphic p.(Asn178Thr) variant is a negative control, MAF: 0.002, 157 hemizygous in gnomAD. **E** Results of *T*-test conducted between pairs of conditions; MO alone vs the all conditions and MO + wt RNA vs all conditions. All variants identified in the families behaved as loss-of-function alleles, while p.(Pro587Arg) is more likely a null allele

RLIM mutant proteins are able to bind REX1 and that the pathogenic variants located in the RING finger domain have a decreased ubiquitin ligase activity.

Absence of functional *rlim* in zebrafish embryos leads to microcephaly not rescued by the human *RLIM* variants

In addition to in vitro assays performed in cells, we investigated the identified RLIM variants in vivo in the developing zebrafish embryos. Given the microcephaly in affected males, we sought to determine whether the zebrafish homolog of human *RLIM*, *rlim*, plays a role during brain development. We asked whether its absence might lead to abnormal head size in our model and, whether the variants identified in our cohort could rescue this phenotype. First, we identified a single *rlim* gene in zebrafish (Ensembl: ENSDART:00000113567.3) with 66% sequence similarity with human *RLIM*. We designed a sb-MO against zebrafish *rlim* and its efficiency was confirmed by RT-PCR (Supplementary Figure 7). We injected the sb-MO into one-to-two cell stage zebrafish embryos. MO-injected embryos were stained and measured for head size at 5 dpf. We observed a significant reduction of the head size in *rlim* morphants compared to controls ($p < 0.001$, $n = 80$–90 embryos per condition; experiment replicated three times; Fig. 4). To test the specificity of the rlim sb-MO, we co-injected the sb-MO along with the human WT *RLIM* mRNA. Compared to sb-MO alone, the co-injection of MO and WT mRNA led to a complete rescue of the head size phenotype ($p < 0.001$ sb-MO alone vs. sb-MO and WT mRNA, Fig. 4) suggesting that the effect of the sb-MO was specific to *rlim* and that the microcephaly was not due to toxicity or off-target effects. To validate our findings, we generated a F0 population of CRISPR mutant *rlim* embryos by introducing small indels in the zebrafish ortholog of *RLIM* using CRISPR/Cas9 genome editing approach. We designed and tested several gRNAs targeting *rlim*. We selected a gRNA that gave 75% of mosaicism in the F0 population as determined by T7 endonuclease I assay followed by Sanger sequencing (see Supplementary Figure 7C). We scored these mutant embryos for head size defects at 5 dpf and found a significant reduction of the head size compared to sham-injected controls ($p < 0.001$, $n =$ 35–40 embryos per condition, three independent experiments) (Fig. 4). The embryos injected with either the gRNA or the Cas9 protein were indistinguishable from controls. These data suggested that *rlim* is required during early brain development in zebrafish embryos. We determined the pathogenicity of the *RLIM* variants found in our cohort. We co-injected *rlim* sb-MO with *RLIM* mRNAs carrying one of the following variants: p.(Pro77Leu), p.(Tyr356Cys), -p.(Arg365Cys), p.(Arg387Cys), p.(Pro587Arg), p.(Arg599Cys), p.(Arg611Cys) and determined whether the mutant mRNAs rescued the microcephaly phenotype induced by the sb-MO. We observed that all seven mutant RNAs failed to rescue the head size phenotype and were likely acting as loss-of-function alleles (Fig. 4). To confirm the specificity of our functional assay, we also tested a common variant in *RLIM* found in the gnomAD database: p.(Asn178Thr) (MAF:0.002, 157 hemizygous individuals). As expected, this variant scored benign in our assay; the p.(Asn178Thr) nonpathogenic polymorphic variant was able to rescue the head size phenotype ($p < 0.001$ compared to sb-MO alone, Fig. 4). Finally, overexpression of the WT or mutant mRNAs alone led to no head size defect, which supported our conclusion that the missense variants more likely act as loss-of-function alleles than having a gain-of-function or dominant negative effect (Supplementary Figure 8). Taken together, our in vivo data showed that absence of functional *rlim* leads to microcephaly and that all seven human *RLIM* variants present in the families failed to rescue head size and are likely loss-of-function alleles. However despite the results obtained in zebrafish, pathogenicity of the p.(Pro77Leu) variant identified in Family A remains uncertain (see Discussion below).

Discussion

The presented families with *RLIM* variants indicate that defective RLIM protein function caused a novel syndromic form of XLID in the affected surviving males. These males have a recognizable facial phenotype, ID, behavioral problems starting at puberty, hypogenitalism, gait problems, short stubby thumbs, and pes planus (Table 1, Fig. 2, Supplementary text, Supplementary Table 1, Supplementary Figure 4, Supplementary Videos 1 and 2). Progressive neurological features such as walking problems evolving to spasticity were noted in affected males with and without seizures. Additional neuroimaging, in particular imaging that is more sensitive to subtle white matter abnormalities, such as FLAIR images (MRI) and PET, will clarify how common the white matter changes are, and whether pituitary atrophy or pineal gland cysts are consistent features of the disorder. Identification of further cases at older ages will determine whether progressive neurological symptoms and neurodegenerative disorders such as Alzheimer dementia occur in *RLIM*-related disorder. Currently, treatment is limited to early intervention, special education, family support and treatment for associated seizure, behavioral, sleep and mental health conditions, as well as recurrence risk counseling.

No particular anti-epileptic medication was found to be consistently more effective in the affected males (Families A, C, D, and F) with seizure disorders, and most affected individuals from Families D and F were seizure free on

medication (e.g., Depakin). For mild spasticity, no treatment was given. However, in the severe case (A.II.2) a baclofen pump eased the spasticity. The psychiatric disorders in the adults, e.g., schizophrenia (C.IV:2) and fear/anxiety (D. III.11) were mainly treated with antipsychotic drugs (e.g., Haldol).

Despite the growing number of families with pathogenic variants in *RLIM*, there is no clear genotype–phenotype correlation appearing. The severely affected boy with the maternally inherited *RLIM* variant (p.(Pro77Leu)) from Family A fits well into the *RLIM* clinical spectrum. However, despite the strongly overlapping clinical features with males who carry a pathogenic variant in *RLIM* and the results obtained in zebrafish, there are several lines of evidence which argue against the pathogenicity of this variant. It was present in only one affected individual, the same variant was identified in two males in gnomAD, the variant did not show a functional effect in the ubiquitination assay and did not cluster with the rest of the RLIM variants. Combined, the pathogenicity of the p.(Pro77Leu) variant identified in Family A remains uncertain until additional similarly affected males with this variant are identified and the mechanism how this variant could cause disease is resolved.

Most non-surviving males and two of three affected fetuses presented with multiple congenital malformations including (relative) microcephaly, CDH with associated LH, urogenital abnormalities, and short terminal phalanges (e.g., stubby thumbs) with or without nail hypoplasia or absent nails. Earlier chromosome studies identified several recurrent deletions in patients with CDH, including, e.g., 1q41-42, 8p23.1, and 15q26. Recently, efforts at identifying other genetic causes using large cohorts of patients with CDH have been made [34, 35] and several critical CDH genes have been identified such as *ZFPM2*, *GATA4*, *GATA6* [36, 37] and rare variants in other genes, e.g., *STAG2* which is implicated in a syndromic form of XLID with microcephaly and a behavioral phenotype [38–40]. Complex disorders including CDH with associated LH (and pulmonary hypertension) include Donnai-Barrow syndrome (LRP2), CHARGE syndrome (CHD7), Matthew-Wood syndrome (STRA6), Simpson-Golabi-Behmel syndrome (GPC3), Cornelia de Lange syndrome (NIPBL), and autosomal recessive Fryns Syndrome (PIGN) [32]. In the past, there have been speculations on an X-linked form of Fryns syndrome. Fryns syndrome is characterized by diaphragmatic defects (diaphragmatic hernia, eventration, hypoplasia, or agenesis); characteristic facial appearance (coarse facies, ocular hypertelorism, broad and flat nasal bridge, thick nasal tip, long philtrum, low-set and poorly formed ears, tented upper lip, macrostomia, micrognathia); distal digital hypoplasia (nails, terminal phalanges); pulmonary hypoplasia; and associated anomalies (polyhydramnios, cloudy corneas, and/or microphthalmia, orofacial clefting, renal dysplasia/renal cortical cysts, and/or malformations involving the brain, cardiovascular system, gastrointestinal system, genitalia) [41]. Comparison between Fryns syndrome and the syndrome associated with *RLIM* variants led us to conclude that both syndromes have congenital malformations in common (See Supplementary Figure 2) except for the facial features and eye abnormalities.

The heterozygous female carriers have normal cognition and behavior, but can have mild skeletal features. We speculate that this might be related to the presence of cells with an inactivated WT X-chromosome, the proportion of which might vary among different females and vary in different tissues of the heterozygous carrier females. POI is a key feature of the RLIM syndrome similar to various other syndromic or non-syndromic forms of POI, including *FMR1* (Xq27.3) pre-mutation, and rare variants in genes affecting the TGF-beta and bone morphogenetic proteins (BMPs) signaling pathway such as *BMP15* (Xp11.22) and *FOXL2* (3q22) [42]. The *RLIM* gene and protein are expressed in follicle cells (http://www.proteinatlas.org/ENSG00000131263-RLIM/tissue) and in these cells the inactive X chromosome is reactivated, which could result in a dominant negative effect or gain-of-function effect of mutant RLIM or in haploinsuffiency. Whether the mutations presented in this study affect human XCI needs further investigation. Notably, *RLIM* variants in all reported families segregated with highly skewed XCI (>95%) in the carrier females with preferential inactivation of the mutant X-chromosome, whereas none of the noncarrier female relatives displayed highly skewed XCI. Highly skewed XCI could be the result of primary or secondary skewing, which we cannot distinguish from our data. Secondary skewing due to cell selection is more frequently observed in heterozygous females from families with X-linked disorders, and points to a more general protein function. In mouse, RLIM was identified as an important *trans*-acting activator of XCI, and mutations lead to primary skewed XCI [14–16, 43]. Primary XCI skewing in humans is very rare. Nevertheless, the involvement of skeletal tissue in Family D, could suggest that the observed XCI is primary, and that RLIM regulates human XCI.

RLIM is an E3 ubiquitin ligase and plays together with other proteins a crucial role within the ubiquitin–proteasome system (UPS), and several ligases and coenzymes within the UPS play an important role in the spatial and temporal control of protein turnover in the nervous system [44]. The UPS regulates the development and maintenance of specialized neuronal structures, and consequently, neuronal transmission. Its dysregulation leads to various movement disturbances, dementia and hypogonadotropic hypogonadism [44, 45]. Thus, it is not surprising that a growing group of ID proteins are directly involved in

UPS-mediated protein degradation, such as UBE3A [46] [47], UBE2A [48, 49, 50, 51], UBE3B [52, 47], HUWE1 [53, 54, 55], MID1 [56–59], CUL4B [60,61–63], UBR1 [64, 65, 66], TRIP12 [67–69], and RNF216 [45,70–72].

Combining our clinical and genetic results with entries in freely accessible databases (e.g., gnomAD, ExAC, Decipher, ClinVar, dbVar), we hypothesize that most likely total loss-of-RLIM function in males is incompatible with life, as reflected by the *RLIM* missense variants causing lethality in some affected males from several families. These missense variants affect highly conserved amino acids and all but one lie within the two RLIM protein domains (Fig. 3A and Supplementary Figure 1).

Rlim is widely expressed in the mouse during embryogenesis and regulates proteins implicated in cellular and developmental processes, including CLIM [8, 9], LMO [8], HDAC2 [73], TRF1 [18], SMAD77 [11], and REX1 [2, 43] through its ubiquitin ligase activity. Strikingly, our in vitro studies examining ubiquitination level of co-expressed REX1, the human counterpart of the well-established RLIM ubiquitin ligase substrate in the mouse, revealed that overexpressed mutant RLIM is able to bind REX1, but all pathogenic variants in the RING-H2 zinc finger of RLIM had highly impaired ubiquitin ligase activity. In contrast mutant RLIM with amino acid changes located outside the RING-H2 zinc finger did not have a major effect on REX1 ubiquitination level. From our clinical data, we observed that variants of the C-terminal RING-H2 zinc finger seem more deleterious than variants located in the RLIM binding region (e.g., severe and lethal affected males in Families E, G, and I).

Although, these studies were performed in vitro and we do not know the consequences of altered ubiquitination of REX1, it is possible that mutant RLIM has an effect on REX1 in vivo. REX1 is expressed in several organs, including the brain, and plays an important role in differentiation, proliferation, and pluripotency. Recent proteomic and network analysis of proteins regulated by REX1 in human embryonic stem cells revealed that it affects several intracellular processes, including translation, regulation of mitochondrial processes, and specific differentiation [74], which might be affected in the patients with RLIM variants.

RLIM/Rlim regulates various other substrates including its interactor Smad7, an important negative regulator of the TGF-beta signaling pathway [75]. RLIM depletion in mammalian cells reduces SMAD7 ubiquitination, thereby stabilizing SMAD7. The resulting accumulation of SMAD7 inhibits TGF-beta signaling by promoting its proteasomal degradation. Conversely, RLIM/Rlim positively regulates activin and BMP/Smad signaling and controls embryonic stem cell fate and morphogenesis by targeting SMAD7/Smad7 for degradation, as shown in both mouse embryonic stem cells and zebrafish embryos [11]. In addition, Rlim antagonizes Smad7 during Nodal-dependent and BMP-dependent signaling and morphogenetic events in early zebrafish development [11]. Although possible effects of mutant human RLIM on TGF-beta and BMP signaling needs more investigation, in humans failure of TGF-beta signaling leads to digit malformation syndromes [76]. Similarly, disturbances of the BMP signaling pathway, which plays multiple roles in nervous system development and differentiation including proper formation of the forebrain, cause various phenotypes similar to the clinical features present in the families with *RLIM* missense variants. For example, BMP4 is involved in lung development, plays an essential role in atrioventricular septation of the heart, is important for complete development of the urethra during embryonic development, forms the precursor germ cell formation to seminal vesicle development and is involved in the generation of preadipocytes from mesenchymal stem cells followed by differentiation into adipocytes [77]. Knockdown of BMP4 in chicken leads to lethal CDH and LH [78]. Four RLIM-affected males presented with CHD resembling CHD types described in the 22q11-deletion syndrome. TBX1, which resides in this 22q11 chromosomal region, is very dose sensitive and is involved in the formation of the secondary heart field together with its targets, e.g., SMAD7 [79], SHH, FGF8 and BMP4 [80], indicating once again the involvement of subtle (dose) dysregulation of RLIM downstream effectors can have consequences for the expression of the clinical phenotype.

A frequent clinical feature of the affected boys is microcephaly. This prompted us to study the variants identified in the families in vivo using zebrafish embryo as a model. Zebrafish has a single *rlim* orthologue. Knockdown of *rlim* in zebrafish using antisense sb-MO or CRISPR/Cas9 genome editing tool caused a statistically significant smaller head size. Co-injection of sb-MO and WT human *RLIM* completely rescued the phenotype. In contrast, none of the variants identified in the families rescued the small head size of zebrafish morphants, thereby further supporting the deleterious nature of the *RLIM* variants. These in vivo data have been further confirmed by an independent study in *Xenopus* where *rlim* knockdown gives rise to mesenchymal small brains, branchial arch and mesonephros malformations [10]. Comparable clinical features are present in some RLIM-affected (non-surviving) males.

RLIM interacts with several pathways involved in normal brain development (SOX [81–83], FGF [84], SHH [85], LHX [8]) and key interactors cause psychiatric disorders. Recently, the transcriptional factor NPAS3 has been identified as a RLIM-interacting protein in neural stem cells [86]. NPAS3 has been associated to psychiatric disorders with several lines of evidence: three nonsynonymous variants in *NPAS3* associated with schizophrenia [87], a balanced chromosome translocation that disrupted *NPAS3*

[87, 88], and, population studies have associated common genetic variants of *NPAS3* [89], bipolar disorder [90], and antipsychotic efficacy [91]. Knockout mice showed behavioral and hippocampal neurogenesis defects consistent with human illness [92]. We speculate that RLIM dysregulation can impair normal NPAS3 function in the adult brain of males with RLIM defects. Furthermore, *Npas3* is expressed in early embryonic lung tissue and *Npas3*-null mice have reduced lung branching morphogenesis but are viable prenatally. Newborns die because of respiratory distress, with decreased *Shh*, *Fgf9*, *Fgf10*, and *Bmp4* mRNAs and increased *Spry2* expression, consistent with reduced FGF signaling [93]. The ubiquitin ligase activity of RLIM is essential for corepressor dependent transcriptional activation of the LIM-HD transcription factors LHX3 and LHX4 [9], which are important for pituitary development, e.g., mutations in human *LHX3* and *LHX4* genes cause combined pituitary hormone deficiency [9]. Furthermore, RLIM acts as a co-regulator of LIM-HD containing transcription factors via the recruitment of the Sin3A/histone deacetylase co-repressor complex. Haploinsufficiency of *SIN3A* causes a recognizable ID syndrome with a subset of the individuals displaying ASD, seizures, microcephaly and short stature [94]. Also, pathogenic variants in the RLIM-interacting protein YY1, a zinc finger transcription factor, which is implicated in the regulation of XCI [2] in mice, cause a syndromic form of ID with behavioral disturbances, intrauterine growth restriction, and various congenital malformations, through dysregulation of key transcriptional regulators [95]. These findings could hint at RLIM-NPAS3, RLIM-SIN3A, and RLIM-YY1 co-regulatory functions that, when impaired by genetic mutations, lead to clinically overlapping neurodevelopmental disorders.

The detailed phenotype analysis of the families with pathogenic variants, or variant of unknown significance in the case of Family A, affecting RLIM's function showed that mutations in this gene cause a recognizable X-linked syndromic disorder. More work is required to understand the pathophysiology of *RLIM*-related conditions in the patients. Our current data suggest that a hypomorphic *RLIM* allele affects the brain and multiple other organs during development with consequences for male offspring. We recommend that *RLIM* be included in panels for pre- and/or postnatal genetic investigation of undiagnosed diaphragmatic hernia, MCA with genital abnormalities, nail hypoplasia and for (syndromic) ID with behavioral problems in males and nonrandom skewing in heterozygous female carriers.

Acknowledgements The authors would like to thank the individuals and their families who participated in this study. We thank Jackie Boyle for her contribution to Family C, Friederike Ruebenstrunk for establishing contact with Family I, and Joop Lavel for technical assistance. The authors would like to thank the Genome Aggregation Database (gnomAD) and the groups that provided exome and genome variant data to this resource. A full list of contributing groups can be found at http://gnomad.broadinstitute.org/about. This study was supported by two Dutch NWO VENI grants: OND1312421 to S.G.M.F. and OND1358237 to C.G.P, the European Union grant QLG3-CT-2002-01810 (EuroMRX Consortium), the EU FP7 project GENCODYS, grant number 241995, Australian NHMRC grants 1091593 and 1041920 to J.G., and the European Commission via its Erasmus Joint Doctoral programme 2013-0040 to M.K. C.G. is a grantee of a NARSAD Young Investigator Grant from the Brain and Behavior Research Foundation.

Compliance with ethical standards

Conflict of interest The authors declare that they have no conflict of interest.

References

1. Retaux S, Bachy I. A short history of LIM domains (1993-2002): from protein interaction to degradation. Mol Neurobiol. 2002;26:269–81.
2. Gontan C, Achame EM, Demmers J, Barakat TS, Rentmeester E, van IW, et al. RNF12 initiates X-chromosome inactivation by targeting REX1 for degradation. Nature. 2012;485:386–90.
3. Hu H, Haas SA, Chelly J, Van Esch H, Raynaud M, de Brouwer AP, et al. X-exome sequencing of 405 unresolved families identifies seven novel intellectual disability genes. Mol Psychiatry. 2016;21:133–48.
4. Tonne E, Holdhus R, Stansberg C, Stray-Pedersen A, Petersen K, Brunner HG, et al. Syndromic X-linked intellectual disability segregating with a missense variant in RLIM. Eur J Hum Genet. 2015;23:1652–6.
5. Rodriguez Criado G. [New X linked mental retardation syndrome]. An De Pediatr. 2012;76:184–191.
6. Gao R, Wang L, Cai H, Zhu J, Yu L. E3 ubiquitin ligase RLIM negatively regulates c-Myc transcriptional activity and restrains cell proliferation. PloS ONE. 2016;11:e0164086.
7. Ostendorff HP, Bossenz M, Mincheva A, Copeland NG, Gilbert DJ, Jenkins NA, et al. Functional characterization of the gene encoding RLIM, the corepressor of LIM homeodomain factors. Genomics. 2000;69:120–30.
8. Bach I, Rodriguez-Esteban C, Carriere C, Bhushan A, Krones A, Rose DW, et al. RLIM inhibits functional activity of LIM homeodomain transcription factors via recruitment of the histone deacetylase complex. Nat Genet. 1999;22:394–9.
9. Ostendorff HP, Peirano RI, Peters MA, Schluter A, Bossenz M, Scheffner M, et al. Ubiquitination-dependent cofactor exchange on LIM homeodomain transcription factors. Nature. 2002;416:99–103.
10. Hiratani I, Yamamoto N, Mochizuki T, Ohmori SY, Taira M. Selective degradation of excess Ldb1 by Rnf12/RLIM confers proper Ldb1 expression levels and Xlim-1/Ldb1 stoichiometry in Xenopus organizer functions. Development. 2003;130:4161–75.
11. Zhang L, Huang H, Zhou F, Schimmel J, Pardo CG, Zhang T, et al. RNF12 controls embryonic stem cell fate and morphogenesis in zebrafish embryos by targeting Smad7 for degradation. Mol Cell. 2012;46:650–61.
12. Shin J, Wallingford MC, Gallant J, Marcho C, Jiao B, Byron M, et al. RLIM is dispensable for X-chromosome inactivation in the mouse embryonic epiblast. Nature. 2014;511:86–89.
13. Ostendorff HP, Tursun B, Cornils K, Schluter A, Drung A, Gungor C, et al. Dynamic expression of LIM cofactors in the developing mouse neural tube. Dev Dyn. 2006;235:786–91.

14. Jonkers I, Barakat TS, Achame EM, Monkhorst K, Kenter A, Rentmeester E, et al. RNF12 is an X-encoded dose-dependent activator of X chromosome inactivation. Cell. 2009;139: 999–1011.
15. Barakat TS, Loos F, van Staveren S, Myronova E, Ghazvini M, Grootegoed JA, et al. The trans-activator RNF12 and cis-acting elements effectuate X chromosome inactivation independent of X-pairing. Mol Cell. 2014;53:965–78.
16. Shin J, Bossenz M, Chung Y, Ma H, Byron M, Taniguchi-Ishigaki N, et al. Maternal Rnf12/RLIM is required for imprinted X-chromosome inactivation in mice. Nature. 2010;467:977–81.
17. Gontan C, Jonkers I, Gribnau J. Long noncoding RNAs and X chromosome inactivation. Prog Mol Subcell Biol. 2011;51:43–64.
18. Her YR, Chung IK. Ubiquitin ligase RLIM modulates telomere length homeostasis through a proteolysis of TRF1. J Biol Chem. 2009;284:8557–66.
19. Chen X, Shen J, Li X, Wang X, Long M, Lin F, et al. Rlim, an E3 ubiquitin ligase, influences the stability of Stathmin protein in human osteosarcoma cells. Cell Signal. 2014;26:1532–8.
20. Gao K, Wang C, Jin X, Xiao J, Zhang E, Yang X, et al. RNF12 promotes p53-dependent cell growth suppression and apoptosis by targeting MDM2 for destruction. Cancer Lett. 2016;375:133–41.
21. Huang Y, Yang Y, Gao R, Yang X, Yan X, Wang C, et al. RLIM interacts with Smurf2 and promotes TGF-beta induced U2OS cell migration. Biochem Biophys Res Commun. 2011;414:181–5.
22. Johnsen SA, Gungor C, Prenzel T, Riethdorf S, Riethdorf L, Taniguchi-Ishigaki N, et al. Regulation of estrogen-dependent transcription by the LIM cofactors CLIM and RLIM in breast cancer. Cancer Res. 2009;69:128–36.
23. Jiao B, Taniguchi-Ishigaki N, Gungor C, Peters MA, Chen YW, Riethdorf S, et al. Functional activity of RLIM/Rnf12 is regulated by phosphorylation-dependent nucleocytoplasmic shuttling. Mol Biol Cell. 2013;24:3085–96.
24. Retterer K, Juusola J, Cho MT, Vitazka P, Millan F, Gibellini F, et al. Clinical application of whole-exome sequencing across clinical indications. Genet Med. 2016;18:696–704.
25. Weese D, Emde AK, Rausch T, Doring A, Reinert K. RazerS--fast read mapping with sensitivity control. Genome Res. 2009;19: 1646–54.
26. Emde AK, Schulz MH, Weese D, Sun R, Vingron M, Kalscheuer VM, et al. Detecting genomic indel variants with exact breakpoints in single- and paired-end sequencing data using SplazerS. Bioinformatics. 2012;28:619–27.
27. Kelly M, Williams R, Aojula A, O'Neill J, Trzinscka Z, Grover L, et al. Peptide aptamers: novel coatings for orthopaedic implants. Mater Sci Eng C Mater Biol Appl. 2015;54:84–93.
28. des Portes V, Beldjord C, Chelly J, Hamel B, Kremer H, Smits A, et al. X-linked nonspecific mental retardation (MRX) linkage studies in 25 unrelated families: the European XLMR consortium. Am J Med Genet. 1999;85:263–5.
29. Frints SG, Borghgraef M, Froyen G, Marynen P, Fryns JP. Clinical study and haplotype analysis in two brothers with Partington syndrome. Am J Med Genet. 2002;112:361–8.
30. Carrel L, Willard HF. An assay for X inactivation based on differential methylation at the fragile X locus, FMR1. Am J Med Genet. 1996;64:27–30.
31. Allen RC, Zoghbi HY, Moseley AB, Rosenblatt HM, Belmont JW. Methylation of HpaII and HhaI sites near the polymorphic CAG repeat in the human androgen-receptor gene correlates with X chromosome inactivation. Am J Hum Genet. 1992;51:1229–39.
32. Westerfield M. The zebrafish book. A guide for the laboratory use of zebrafish (*Danio rerio*). 3rd ed., vol. 385. Eugene, OR: University of Oregon Press; 1995.
33. Jao LE, Wente SR, Chen W. Efficient multiplex biallelic zebrafish genome editing using a CRISPR nuclease system. Proc Natl Acad Sci USA. 2013;110:13904–9.
34. Donahoe PK, Longoni M, High FA. Polygenic causes of congenital diaphragmatic hernia produce common lung pathologies. Am J Pathol. 2016;186:2532–43.
35. Yu L, Sawle AD, Wynn J, Aspelund G, Stolar CJ, Arkovitz MS, et al. Increased burden of de novo predicted deleterious variants in complex congenital diaphragmatic hernia. Hum Mol Genet. 2015;24:4764–73.
36. Longoni M, High FA, Qi H, Joy MP, Hila R, Coletti CM, et al. Genome-wide enrichment of damaging de novo variants in patients with isolated and complex congenital diaphragmatic hernia. Hum Genet. 2017;136:679–91.
37. Longoni M, High FA, Russell MK, Kashani A, Tracy AA, Coletti CM, et al. Molecular pathogenesis of congenital diaphragmatic hernia revealed by exome sequencing, developmental data, and bioinformatics. Proc Natl Acad Sci USA. 2014;111:12450–5.
38. Mullegama SV, Klein SD, Mulatinho MV, Senaratne TN, Singh K, Center UCG, et al. De novo loss-of-function variants in STAG2 are associated with developmental delay, microcephaly, and congenital anomalies. Am J Med Genet A. 2017;173: 1319–27.
39. Kumar R, Corbett MA, Van Bon BW, Gardner A, Woenig JA, Jolly LA, et al. Increased STAG2 dosage defines a novel cohesinopathy with intellectual disability and behavioral problems. Hum Mol Genet. 2015;24:7171–81.
40. Yingjun X, Wen T, Yujian L, Lingling X, Huimin H, Qun F, et al. Microduplication of chromosome Xq25 encompassing STAG2 gene in a boy with intellectual disability. Eur J Med Genet. 2015;58:116–21.
41. Bone KM, Chernos JE, Perrier R, Innes AM, Bernier FP, McLeod R, et al. Mosaic trisomy 1q: a recurring chromosome anomaly that is a diagnostic challenge and is associated with a Fryns-like phenotype. Prenat Diagn. 2017;37:602–10.
42. Rossetti R, Ferrari I, Bonomi M, Persani L. Genetics of primary ovarian insufficiency. Clin Genet. 2017;91:183–98.
43. Bach I. Releasing the break on X chromosome inactivation: Rnf12/RLIM targets REX1 for degradation. Cell Res. 2012;22: 1524–6.
44. Upadhyay A, Joshi V, Amanullah A, Mishra R, Arora N, Prasad A, et al. E3 ubiquitin ligases neurobiological mechanisms: development to degeneration. Front Mol Neurosci. 2017;10:151.
45. Margolin DH, Kousi M, Chan YM, Lim ET, Schmahmann JD, Hadjivassiliou M, et al. Ataxia, dementia, and hypogonadotropism caused by disordered ubiquitination. N Engl J Med. 2013;368: 1992–2003.
46. Kishino T, Lalande M, Wagstaff J. UBE3A/E6-AP mutations cause Angelman syndrome. Nat Genet. 1997;15:70–73.
47. Basel-Vanagaite L, Dallapiccola B, Ramirez-Solis R, Segref A, Thiele H, Edwards A, et al. Deficiency for the ubiquitin ligase UBE3B in a blepharophimosis-ptosis-intellectual-disability syndrome. Am J Hum Genet. 2012;91:998–1010.
48. Nascimento RM, Otto PA, de Brouwer AP, Vianna-Morgante AM. UBE2A, which encodes a ubiquitin-conjugating enzyme, is mutated in a novel X-linked mental retardation syndrome. Am J Hum Genet. 2006;79:549–55.
49. Budny B, Badura-Stronka M, Materna-Kiryluk A, Tzschach A, Raynaud M, Latos-Bielenska A, et al. Novel missense mutations in the ubiquitination-related gene UBE2A cause a recognizable X-linked mental retardation syndrome. Clin Genet. 2010;77:541–51.
50. Vandewalle J, Bauters M, Van Esch H, Belet S, Verbeeck J, Fieremans N, et al. The mitochondrial solute carrier SLC25A5 at Xq24 is a novel candidate gene for non-syndromic intellectual disability. Hum Genet. 2013;132:1177–85.
51. Haddad DM, Vilain S, Vos M, Esposito G, Matta S, Kalscheuer VM, et al. Mutations in the intellectual disability gene Ube2a cause neuronal dysfunction and impair parkin-dependent mitophagy. Mol Cell. 2013;50:831–43.

52. Flex E, Ciolfi A, Caputo V, Fodale V, Leoni C, Melis D, et al. Loss of function of the E3 ubiquitin-protein ligase UBE3B causes Kaufman oculocerebrofacial syndrome. J Med Genet. 2013;50:493–9.
53. Isrie M, Kalscheuer VM, Holvoet M, Fieremans N, Van Esch H, Devriendt K. HUWE1 mutation explains phenotypic severity in a case of familial idiopathic intellectual disability. Eur J Med Genet. 2013;56:379–82.
54. Froyen G, Belet S, Martinez F, Santos-Reboucas CB, Declercq M, Verbeeck J, et al. Copy-number gains of HUWE1 due to replication- and recombination-based rearrangements. Am J Hum Genet. 2012;91:252–64.
55. Froyen G, Corbett M, Vandewalle J, Jarvela I, Lawrence O, Meldrum C, et al. Submicroscopic duplications of the hydroxysteroid dehydrogenase HSD17B10 and the E3 ubiquitin ligase HUWE1 are associated with mental retardation. Am J Hum Genet. 2008;82:432–43.
56. So J, Suckow V, Kijas Z, Kalscheuer V, Moser B, Winter J, et al. Mild phenotypes in a series of patients with Opitz GBBB syndrome with MID1 mutations. Am J Med Genet A. 2005;132A:1–7.
57. Quaderi NA, Schweiger S, Gaudenz K, Franco B, Rugarli EI, Berger W, et al. Opitz G/BBB syndrome, a defect of midline development, is due to mutations in a new RING finger gene on Xp22. Nat Genet. 1997;17:285–91.
58. Trockenbacher A, Suckow V, Foerster J, Winter J, Krauss S, Ropers HH, et al. MID1, mutated in Opitz syndrome, encodes an ubiquitin ligase that targets phosphatase 2A for degradation. Nat Genet. 2001;29:287–94.
59. Schweiger S, Dorn S, Fuchs M, Kohler A, Matthes F, Muller EC, et al. The E3 ubiquitin ligase MID1 catalyzes ubiquitination and cleavage of Fu. J Biol Chem. 2014;289:31805–17.
60. Zou Y, Liu Q, Chen B, Zhang X, Guo C, Zhou H, et al. Mutation in CUL4B, which encodes a member of cullin-RING ubiquitin ligase complex, causes X-linked mental retardation. Am J Hum Genet. 2007;80:561–6.
61. Vulto-van Silfhout AT, Nakagawa T, Bahi-Buisson N, Haas SA, Hu H, Bienek M, et al. Variants in CUL4B are associated with cerebral malformations. Hum Mutat. 2015;36:106–17.
62. Badura-Stronka M, Jamsheer A, Materna-Kiryluk A, Sowinska A, Kiryluk K, Budny B, et al. A novel nonsense mutation in CUL4B gene in three brothers with X-linked mental retardation syndrome. Clin Genet. 2010;77:141–4.
63. Tarpey PS, Raymond FL, O'Meara S, Edkins S, Teague J, Butler A, et al. Mutations in CUL4B, which encodes a ubiquitin E3 ligase subunit, cause an X-linked mental retardation syndrome associated with aggressive outbursts, seizures, relative macrocephaly, central obesity, hypogonadism, pes cavus, and tremor. Am J Hum Genet. 2007;80:345–52.
64. Hwang CS, Sukalo M, Batygin O, Addor MC, Brunner H, Aytes AP, et al. Ubiquitin ligases of the N-end rule pathway: assessment of mutations in UBR1 that cause the Johanson-Blizzard syndrome. PLoS ONE. 2011;6:e24925.
65. Sukalo M, Fiedler A, Guzman C, Spranger S, Addor MC, McHeik JN, et al. Mutations in the human UBR1 gene and the associated phenotypic spectrum. Hum Mutat. 2014;35:521–31.
66. Zenker M, Mayerle J, Lerch MM, Tagariello A, Zerres K, Durie PR, et al. Deficiency of UBR1, a ubiquitin ligase of the N-end rule pathway, causes pancreatic dysfunction, malformations and mental retardation (Johanson-Blizzard syndrome). Nat Genet. 2005;37:1345–50.
67. Zhang J, Gambin T, Yuan B, Szafranski P, Rosenfeld JA, Balwi MA, et al. Erratum to: Haploinsufficiency of the E3 ubiquitin-protein ligase gene TRIP12 causes intellectual disability with or without autism spectrum disorders, speech delay, and dysmorphic features. Hum Genet. 2017;136:1009–11.
68. Zhang J, Gambin T, Yuan B, Szafranski P, Rosenfeld JA, Balwi MA, et al. Haploinsufficiency of the E3 ubiquitin-protein ligase gene TRIP12 causes intellectual disability with or without autism spectrum disorders, speech delay, and dysmorphic features. Hum Genet. 2017;136:377–86.
69. Bramswig NC, Ludecke HJ, Pettersson M, Albrecht B, Bernier RA, Cremer K, et al. Identification of new TRIP12 variants and detailed clinical evaluation of individuals with non-syndromic intellectual disability with or without autism. Hum Genet. 2017;136:179–92.
70. Alqwaifly M, Bohlega S. Ataxia and hypogonadotropic hypogonadism with intrafamilial variability caused by RNF216 mutation. Neurol Int. 2016;8:6444.
71. Ganos C, Hersheson J, Adams M, Bhatia KP, Houlden H. Syndromic associations and RNF216 mutations. Park Relat Disord. 2015;21:1389–90.
72. Santens P, Van Damme T, Steyaert W, Willaert A, Sablonniere B, De Paepe A, et al. RNF216 mutations as a novel cause of autosomal recessive Huntington-like disorder. Neurology. 2015;84:1760–6.
73. Kramer OH, Zhu P, Ostendorff HP, Golebiewski M, Tiefenbach J, Peters MA, et al. The histone deacetylase inhibitor valproic acid selectively induces proteasomal degradation of HDAC2. EMBO J. 2003;22:3411–20.
74. Son MY, Kwak JE, Kim YD, Cho YS. Proteomic and network analysis of proteins regulated by REX1 in human embryonic stem cells. Proteomics. 2015;15:2220–9.
75. Hill CS. Inhibiting the inhibitor: the role of RNF12 in TGF-beta superfamily signaling. Mol Cell. 2012;46:558–9.
76. Stricker S, Mundlos S. Mechanisms of digit formation: human malformation syndromes tell the story. Dev Dyn. 2011;240:990–1004.
77. Wang RN, Green J, Wang Z, Deng Y, Qiao M, Peabody M, et al. Bone Morphogenetic Protein (BMP) signaling in development and human diseases. Genes Dis. 2014;1:87–105.
78. Emmerton-Coughlin HM, Martin KK, Chiu JS, Zhao L, Scott LA, Regnault TR, et al. BMP4 and LGL1 are down regulated in an ovine model of congenital diaphragmatic hernia. Front Surg. 2014;1:44.
79. Papangeli I, Scambler PJ. Tbx1 genetically interacts with the transforming growth factor-beta/bone morphogenetic protein inhibitor Smad7 during great vessel remodeling. Circ Res. 2013;112:90–102.
80. Mesbah K, Rana MS, Francou A, van Duijvenboden K, Papaioannou VE, Moorman AF, et al. Identification of a Tbx1/Tbx2/Tbx3 genetic pathway governing pharyngeal and arterial pole morphogenesis. Hum Mol Genet. 2012;21:1217–29.
81. Weider M, Wegner M. SoxE factors: transcriptional regulators of neural differentiation and nervous system development. Semin Cell Dev Biol. 2017;63:35–42.
82. Sha L, MacIntyre L, Machell JA, Kelly MP, Porteous DJ, Brandon NJ, et al. Transcriptional regulation of neurodevelopmental and metabolic pathways by NPAS3. Mol Psychiatry. 2012;17:267–79.
83. Navarro P, Moffat M, Mullin NP, Chambers I. The X-inactivation trans-activator Rnf12 is negatively regulated by pluripotency factors in embryonic stem cells. Human Genet. 2011;130:255–64.
84. Marie PJ, Debiais F, Hay E. Regulation of human cranial osteoblast phenotype by FGF-2, FGFR-2 and BMP-2 signaling. Histol Histopathol. 2002;17:877–85.
85. Ishibashi M, Saitsu H, Komada M, Shiota K. Signaling cascade coordinating growth of dorsal and ventral tissues of the vertebrate brain, with special reference to the involvement of Sonic Hedgehog signaling. Anat Sci Int. 2005;80:30–36.
86. Moen MJ, Adams HH, Brandsma JH, Dekkers DH, Akinci U, Karkampouna S, et al. An interaction network of mental disorder proteins in neural stem cells. Transl Psychiatry. 2017;7:e1082.

87. Yu L, Arbez N, Nucifora LG, Sell GL, Delisi LE, Ross CA, et al. A mutation in NPAS3 segregates with mental illness in a small family. Mol Psychiatry. 2014;19:7–8.
88. Nucifora LG, Wu YC, Lee BJ, Sha L, Margolis RL, Ross CA, et al. A mutation in NPAS3 that segregates with schizophrenia in a small family leads to protein aggregation. Mol Neuropsychiatry. 2016;2:133–44.
89. Pickard BS, Christoforou A, Thomson PA, Fawkes A, Evans KL, Morris SW, et al. Interacting haplotypes at the NPAS3 locus alter risk of schizophrenia and bipolar disorder. Mol Psychiatry. 2009;14:874–84.
90. Ferreira MA, O'Donovan MC, Meng YA, Jones IR, Ruderfer DM, Jones L, et al. Collaborative genome-wide association analysis supports a role for ANK3 and CACNA1C in bipolar disorder. Nat Genet. 2008;40:1056–8.
91. Lavedan C, Licamele L, Volpi S, Hamilton J, Heaton C, Mack K, et al. Association of the NPAS3 gene and five other loci with response to the antipsychotic iloperidone identified in a whole genome association study. Mol Psychiatry. 2009;14:804–19.
92. Erbel-Sieler C, Dudley C, Zhou Y, Wu X, Estill SJ, Han T, et al. Behavioral and regulatory abnormalities in mice deficient in the NPAS1 and NPAS3 transcription factors. Proc Natl Acad Sci USA. 2004;101:13648–53.
93. Zhou S, Degan S, Potts EN, Foster WM, Sunday ME. NPAS3 is a trachealess homolog critical for lung development and homeostasis. Proc Natl Acad Sci USA. 2009;106:11691–6.
94. Witteveen JS, Willemsen MH, Dombroski TC, van Bakel NH, Nillesen WM, van Hulten JA, et al. Haploinsufficiency of MeCP2-interacting transcriptional co-repressor SIN3A causes mild intellectual disability by affecting the development of cortical integrity. Nat Genet. 2016;48:877–87.
95. Gabriele M, Vulto-van Silfhout AT, Germain PL, Vitriolo A, Kumar R, Douglas E, et al. YY1 haploinsufficiency causes an intellectual disability syndrome featuring transcriptional and chromatin dysfunction. Am J Hum Genet. 2017;100:907–25.

Affiliations

Suzanna G. M. Frints[1,2] · Aysegul Ozanturk[3] · Germán Rodríguez Criado[4] · Ute Grasshoff[5] · Bas de Hoon[6,7] · Michael Field[8] · Sylvie Manouvrier-Hanu[9,10] · Scott E. Hickey[11,12] · Molka Kammoun[13] · Karen W. Gripp[14] · Claudia Bauer[5] · Christopher Schroeder[5] · Annick Toutain[15,16] · Theresa Mihalic Mosher[11,12,17] · Benjamin J. Kelly[17] · Peter White[12,17] · Andreas Dufke[5] · Eveline Rentmeester[6] · Sungjin Moon[3] · Daniel C Koboldt[12,17] · Kees E. P. van Roozendaal[1,2] · Hao Hu[18] · Stefan A. Haas[19] · Hans-Hilger Ropers[18] · Lucinda Murray[8] · Eric Haan[20,21] · Marie Shaw[20] · Renee Carroll[20] · Kathryn Friend[22] · Jan Liebelt[21] · Lynne Hobson[22] · Marjan De Rademaeker[23] · Joep Geraedts[1,2] · Jean-Pierre Fryns[13] · Joris Vermeesch[13] · Martine Raynaud[15,16] · Olaf Riess[5] · Joost Gribnau[6] · Nicholas Katsanis[3] · Koen Devriendt[13] · Peter Bauer[5] · Jozef Gecz[20,24] · Christelle Golzio[3,25] · Cristina Gontan[6] · Vera M. Kalscheuer[26]

[1] Department of Clinical Genetics, Maastricht University Medical Center+, azM, Maastricht 6202 AZ, The Netherlands

[2] Department of Genetics and Cell Biology, School for Oncology and Developmental Biology, GROW, FHML, Maastricht University, Maastricht 6200 MD, The Netherlands

[3] Center for Human Disease Modeling and Departments of Pediatrics and Psychiatry, Duke University, Durham, NC 27710, USA

[4] Unidad de Genética Clínica, Hospital Virgen del Rocío, Sevilla 41920, Spain

[5] Institute of Medical Genetics and Applied Genomics, University of Tübingen, Tübingen 72076, Germany

[6] Department of Developmental Biology, Erasmus University Medical Center, Rotterdam 3015 CN Rotterdam, The Netherlands

[7] Department of Gynaecology and Obstetrics, Erasmus University Medical Center, Rotterdam 3015 CN, The Netherlands

[8] GOLD (Genetics of Learning and Disability) Service, Hunter Genetics, Waratah, NSW 2298, Australia

[9] Clinique de Génétique médicale Guy Fontaine, Centre de référence maladies rares Anomalies du développement Hôpital Jeanne de Flandre, Lille 59000, France

[10] EA 7364 RADEME Maladies Rares du Développement et du Métabolisme, Faculté de Médecine, Université de Lille, Lille 59000, France

[11] Division of Molecular & Human Genetics, Nationwide Children's Hospital, Columbus, OH 43205, USA

[12] Department of Pediatrics, The Ohio State University College of Medicine, Columbus, OH 43205, USA

[13] Center for Human Genetics, University Hospitals Leuven, Leuven 3000, Belgium

[14] Alfred I. duPont Hospital for Children Nemours, Wilmington, DE 19803, USA

[15] Service de Génétique, Hôpital Bretonneau, CHU de Tours, Tours 37044, France

[16] UMR 1253, iBrain, Université de Tours, Inserm, Tours 37032, France

[17] The Institute for Genomic Medicine, Nationwide Children's Hospital, Columbus, OH 43205, USA

[18] Department of Human Molecular Genetics, Max Planck Institute for Molecular Genetics, Berlin 14195, Germany

[19] Department of Computational Molecular Biology, Max Planck Institute for Molecular Genetics, Berlin 14195, Germany

[20] Adelaide Medical School and Robinson Research Institute, The University of Adelaide, Adelaide, SA 5000, Australia

[21] South Australian Clinical Genetics Service, SA Pathology (at

Women's and Children's Hospital), North Adelaide, SA 5006, Australia

[22] Genetics and Molecular Pathology, SA Pathology, Adelaide, SA 5006, Australia

[23] Centre for Medical Genetics, Reproduction and Genetics, Reproduction Genetics and Regenerative Medicine, Vrije Universiteit Brussel (VUB), UZ Brussel, 1090 Brussels, Belgium

[24] South Australian Health and Medical Research Institute, Adelaide, SA 5000, Australia

[25] Institut de Génétique et de Biologie Moléculaire et Cellulaire, Department of Translational Medicine and Neurogenetics; Centre National de la Recherche Scientifique, UMR7104; Institut National de la Santé et de la Recherche Médicale, U964, Université de Strasbourg, 67400 Illkirch, France

[26] Research Group Development and Disease, Max Planck Institute for Molecular Genetics, Berlin 14195, Germany